eprints@whiterose.ac.uk
https://eprints.whiterose.ac.uk/

MAGNETOHYDROSTATIC EQUILIBRIUM. II. THREE-DIMENSIONAL MULTIPLE OPEN MAGNETIC FLUX TUBES IN THE STRATIFIED SOLAR ATMOSPHERE

F. A. GENT[1], V. FEDUN[2] AND R. ERDÉLYI[1]

[1]SP²RC, School of Mathematics and Statistics, University of Sheffield, S3 7RH, UK: f.gent@shef.ac.uk and
[2]Space Systems Laboratory, Department of Automatic Control and Systems Engineering, University of Sheffield, S1 3JD, UK

Draft version June 16, 2014

ABSTRACT

A system of multiple open magnetic flux tubes spanning the solar photosphere and lower corona is modeled analytically, within a realistic stratified atmosphere subject to solar gravity. This extends results for a single magnetic flux tube in magnetohydrostatic equilibrium, described in Gent et al. (MNRAS, **435**, 689, 2013). Self-similar magnetic flux tubes are combined to form magnetic structures, which are consistent with high-resolution observations. The observational evidence supports the existence of strands of open flux tubes and loops persisting in a relatively steady state. Self-similar magnetic flux tubes, for which an analytic solution to the plasma density and pressure distribution is possible, are combined. We calculate the appropriate balancing forces, applying to the equations of momentum and energy conservation to preserve equilibrium.

Multiplex flux tube configurations are observed to remain relatively stable for up to a day or more, and it is our aim to apply our model as the background condition for numerical studies of energy transport mechanisms from the solar surface to the corona. We apply magnetic field strength, plasma density, pressure and temperature distributions consistent with observational and theoretical estimates for the lower solar atmosphere. Although each flux tube is identical in construction apart from the location of the radial axis, combinations can be applied to generate a non-axisymmetric magnetic field with multiple non-uniform flux tubes. This is a considerable step forward in modeling the realistic magnetized three-dimensional equilibria of the solar atmosphere.

Subject headings: instabilities — magnetic fields — magnetohydrodynamics (MHD) — Sun:atmosphere — Sun: chromosphere — Sun: transition region

1. INTRODUCTION

At a radius $R_\odot \simeq 696$ Mm from the Sun's core its luminous surface, the photosphere, has a typical temperature of about 6500 K. Based on estimates from semi-empirical 1D models at $h \simeq 0.35$–0.65 Mm above this surface, the temperature falls to a minimum $T \simeq 4200$ K. The temperature then rises with height and experiences rapid jumps to 10^5 K just above $h \simeq 2$ Mm and to 10^6 K beyond $h \simeq 2.5$ Mm (Vernazza et al. 1981; Priest 2000; Aschwanden 2005; Erdélyi 2008, and references therein). The mechanism of heating the solar corona is not well understood. The solar atmosphere is highly active. Jets, flares, prominences, spicules and flux emergence, among others, carry mass and energy from the surface into the atmosphere. Although frequent and powerful, these solar accumulated events do not yet appear to be of sufficient energy to explain the consistently high temperatures for the corona (Zirker 1993; Aschwanden 2005; Klimchuk 2006). An alternative view may be that solar magnetic field lines, in the form of magnetic *flux tubes*, act as guides for magnetohydrodynamic (MHD) waves that may carry the missing energy to heat the corona to observed temperatures (Jess et al. 2007; Morton et al. 2012; Wedemeyer-Böhm et al. 2012)

Coronal loops, comprising strongly magnetized flux tubes, permeate the atmosphere. Given the very low thermal pressure in the solar corona, the magnetic pressure can become dynamically dominant. From the photosphere to the lower corona, there is a drop of six orders of magnitude in the plasma pressure and nine orders of magnitude in the plasma density (Vernazza et al. 1981). Just above 2 Mm from the photosphere there is a transition zone, called the Transition Region (TR), where there is a jump in plasma density and temperature of two orders of magnitude, evident in the black

lines of Figure 1 (see also Figure 1 of Gent et al. 2013, hereafter referred to as Paper I).

Typical footpoint strengths of 100 mT (1000 G) are observed for magnetic flux tubes emerging from the photosphere (Zwaan 1978; Priest 2000; Aschwanden 2005; Erdélyi 2008, and references therein, the latter Chapter 8.7, Chapter 5, respectively). An isolated magnetic flux tube must therefore expand exponentially in radius as it approaches the TR to balance the plasma pressure. Environments with such large dynamical scales are highly challenging to model (DeForest 2007).

Although on some solar timescales they may be regarded as transient features, magnetic flux loops persist in relative pressure equilibrium with the ambient atmosphere for many minutes, days or longer (McGuire et al. 1977; Levine & Withbroe 1977; Malherbe et al. 1983). Let us consider the magnetic field as a wave guide for carrying energy from the lower solar atmosphere and releasing it as heat high in the corona. We can take advantage of the steady background state of the magnetic field and plasma to investigate such transport mechanisms with a series of numerical simulations (Shelyag et al. 2008; Fedun et al. 2009; Shelyag et al. 2009; Fedun et al. 2011a; Vigeesh et al. 2012; Khomenko & Collados 2012; Mumford et al. 2014).

Magnetic flux tubes appear to exhibit overdense cores in the corona, in apparent contradiction with hydrostatic equilibrium (Aschwanden et al. 2001; Winebarger et al. 2003). Modeling a single flux tube in pressure equilibrium for the corona dictates that the internal magnetic pressure arising from a predominantly parallel field will reduce the plasma pressure and, consequently, also plasma density or temperature. Combining multiple flux tubes may induce magnetic tension forces restoring and potentially even enhancing plasma density within the

flux tubes. Figure 1(a) displays the axial profile for the plasma pressure, temperature and density with the same parameters for the magnetic flux tube as applied in Paper I, but with some revisions as outlined in Section 2. Significantly, in the corona, the plasma density inside the flux tube is lower than the ambient plasma. Note that a more gradual expansion of the flux tube is applied (panel (b), below $1\,\mathrm{Mm}$, blue, dashed line). The resulting plasma density, and, to some extent, the pressure, is enhanced in the chromosphere and TR, where there are strong tension forces applying, but not in the corona where the field lines are predominantly parallel.
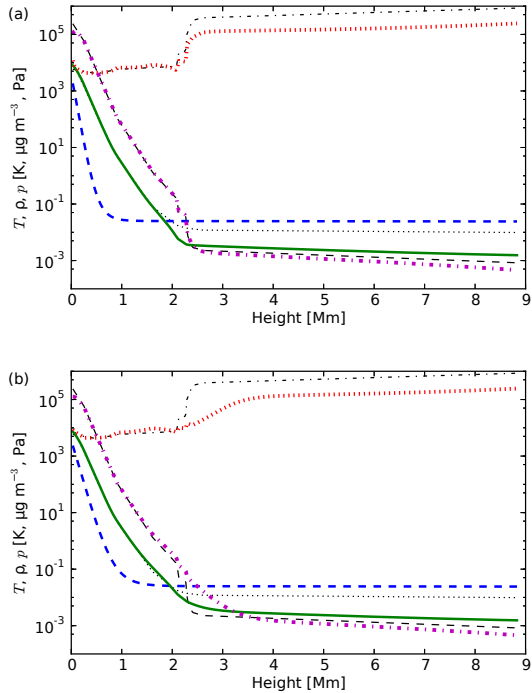

FIG. 1.— 1D-slices along the axis of a single magnetic flux tube for thermal p [Pa] (solid, green) and magnetic $B^2/(2\mu_0)$ [Pa] (dashed, blue) pressure, temperature T [K] (dotted, red) and plasma density ρ [μg m^{-3}] (dash-dotted, purple). Panel (a) has parameters matching Paper I, while (b) applies a reduced expansion rate for the flux tube in the chromosphere. Interpolated 1D fits to the vertical atmospheric profile are shown in black lines (Vernazza et al. 1981; McWhirter et al. 1975, former up to $2.3\,\mathrm{Mm}$; latter above $2.4\,\mathrm{Mm}$). Differences between model and reference profiles vanish away from the flux tube axis.

Numerical models with a single flux tube may miss some of the interesting non-linear effects arising from interactions between neighboring flux tubes. Khomenko et al. (2008); Khomenko & Collados (2012) have constructed a two-dimensional (2D) magnetic field with multiple flux tubes for a domain which does not include the transition region and where each flux tube is identical to its neighbor. Hasan et al. (2005); Hasan & van Ballegooijen (2008) have constructed a 2D magnetic field which does extend into the low corona. In this paper, in a domain from the photosphere to beyond the TR, we construct a three-dimensional (3D) magnetic field with inhomogeneous multiple flux tubes. This is a considerable step forward in realistic modeling of 3D magnetic networks embedded in the highly stratified solar atmosphere.

In a series of papers, Low (e.g., 1985, 1988) describes a method for deriving analytically the equilibrium plasma pressure and density distribution for a set of magnetic field configurations. This result was applied to the global so-lar magnetic field structure and coronal mass ejections (e.g., Tsinganos & Low 1989; Gibson & Low 1998).

Here, we describe an alternative, empirical method for constructing an equilibrium magnetic field comprising multiple non-uniform flux tubes within a realistic stratified solar atmosphere. Our aim is to analytically describe a structure for the magnetic field, matching observational models (e.g., López Fuentes et al. 2008; Kontar et al. 2008; Verth et al. 2011; Jeffrey & Kontar 2013). We derive analytic expressions for adjustments to the plasma pressure and density, due to the magnetic field, to restore pressure balance, also constrained by observational parameters. We empirically identify the minimal balancing forces applying to the MHD equations of momentum and energy conservation that preserve this equilibrium.

The paper is organized as follows. Section 2.1 clarifies what changes have been introduced in comparison to the single magnetic flux tube model detailed in Gent et al. (2013). Section 2.2 describes how the MHD equations governing the perturbed system must be framed to account for the steady background utilizing multiple flux tubes of the form defined in Section 2.3. Section 2.4 outlines how the atmosphere is adjusted to balance the magnetic pressure and tension forces and identifies the balancing forces which must also be applied. In Section 2.5, the changes to the MHD equations are identified. Section 2.6 has examples of heterogeneous multiple flux tube fields that are possible with this method. A summary of the results are presented in Section 3 with some points for discussion. In the Appendix, we show some of the analytic calculations in more detail. For pairs of interacting magnetic flux tubes Appendix A.1 demonstrates why a balancing force must be present in addition to any changes to the plasma pressure and density, and identifies these forces. Profiles for the plasma pressure and density are derived in Appendix A.2.

2. MULTIPLE OPEN MAGNETIC FLUX TUBES

2.1. *Development Beyond the Single Flux Tube Model*

Following Gent et al. (2013) we apply a background atmosphere derived by a combination of modeling profiles from Vernazza et al. (1981, Table 12, VALIIIC) and McWhirter et al. (1975, Table 3) for the chromosphere and lower solar corona, respectively, assuming background equilibrium parameters for the quiet Sun. The profiles interpolated as a function of height above the photosphere are included in Figure 1 as black dotted lines (pressure), dashed (density), and dash-dotted (temperature). Up to the TR, at around $2.2\,\mathrm{Mm}$, the steep pressure and corresponding density gradients dictate that magnetic flux tubes expand rapidly in radius and reduce in flux density. In the solar corona, the flux tube radius is almost steady with height. Our models, both for the single tube and the multiple configurations, capture the reference data profiles very effectively. However, the models do not depend on the choice of atmosphere and the derivation described could be applied to many alternative atmospheric models.

In constructing the magnetic field, we include a constituent to represent an ambient magnetic field, ubiquitous within the solar atmosphere. In Paper I the ambient field was a function of r and z. Here we apply a constant vertical ambient field, which still satisfies the divergence free condition and, as constructed, retains thermal pressure $p > 0$ as $z \to \infty$. The resulting derivatives therefore somewhat simplify, compared to Paper I.

For an axially symmetric flux tube, it is convenient to work

in polar coordinates. This is applied in Paper I and for the individual flux tube element of Appendix A.2 in this paper. For a pair of flux tubes that differ by axial coordinates, however, axial symmetry is broken. In this paper, it is therefore, more convenient to compute the flux tube interactions in Cartesian coordinates.

In Equation (7) for pressure balance the magnetic tension force is of opposite sign to the gradients of pressure. In Paper I the tension force has the wrong sign. The derivations remain valid. With the sign corrected, the flux tube axial plasma density is no longer enhanced in the corona, although it is in the chromosphere, where the tension forces are strongest. This suggests that the enhanced density observed in steady flux tubes may be due to the magnetic tension forces governed by the curvature of the magnetic field lines.

With the pressure and tension forces correctly in opposition, there is much more latitude in the model parameters. The thickness of the flux tube can extend to over $1\,\mathrm{Mm}$, with an upper bound on the footpoint field strength near $150\,\mathrm{mT}$ without negative pressure or density resulting. Solar magnetic flux tubes are unlikely to exhibit such homogeneity. Combining many small uniform flux tubes in non-uniform distribution, we may construct large heterogeneous flux tubes.

2.2. *The MHD Equations*

A motivation for the current work is to facilitate an MHD solution in an environment that includes a plasma density gradient with nine orders of magnitude over a relatively short vertical span. By confining this and other large gradients within a static background, the MHD equations can be re-framed with respect to the significantly more modest differentials of the perturbations.

This article employs several subscripts and superscripts. Subscripts $i, j \in \{1, 2, 3\}$ denote general vector or tensor coordinate components only. The convention of a sum over all three components applies for a repeated index in a single expression. In Cartesian coordinates $x_i = (x_1, x_2, x_3) = (x, y, z)$, and where x, y or z appear as subscripts they refer only to the respective component x_1, x_2 or x_3.

The governing equations of full ideal compressible MHD in their conservative form are:

$$\frac{\partial \rho}{\partial t} + \frac{\partial}{\partial x_i}(\rho u_i) = 0, \qquad (1)$$

$$\frac{\partial(\rho u_i)}{\partial t} + \frac{\partial}{\partial x_j}\left(\rho u_i u_j - \frac{B_i B_j}{\mu_0}\right) + \frac{\partial p_T}{\partial x_i} = \rho g_i, \quad (2)$$

$$\frac{\partial e}{\partial t} + \frac{\partial}{\partial x_i}(e u_i + p_T u_i) - \frac{\partial}{\partial x_j}\left(\frac{B_i B_j u_i}{\mu_0}\right) = \rho g_i u_i, \quad (3)$$

$$\frac{\partial B_i}{\partial t} + \frac{\partial}{\partial x_j}(u_i B_j - u_j B_i) = 0_i, \qquad (4)$$

$$p_T = p + \frac{B_j B_j}{2\mu_0}, \quad p = (\gamma - 1)\left(e - \frac{\rho u_j u_j}{2} - \frac{B_j B_j}{2\mu_0}\right), (5)$$

where ρ is plasma density, and ∇, $\boldsymbol{u}$, $\boldsymbol{B}$ and $\boldsymbol{g}$ are the gradient, velocity, magnetic field, and gravitational acceleration vectors, respectively. e is the total energy density, p is the thermal pressure, p_T is the total pressure (magnetic + thermal), and γ is the adiabatic index of the plasma and μ_0 vacuum magnetic permeability.

Following the approach of Shelyag et al. (2008), we derive the system of equations governing the perturbed MHD vari-

ables. The variables ρ, e, and $\boldsymbol{B}$ are split into their background and perturbed components

$$\rho = \rho_b + \tilde{\rho}, \quad e = e_b + \tilde{e}, \quad \boldsymbol{B} = \boldsymbol{B}_b + \tilde{\boldsymbol{B}}, \qquad (6)$$

where the tilde denotes the perturbed portion and it is assumed ρ_b, e_b and $\boldsymbol{B}_b$ do not vary with time. The subscript b denotes background, and in combination with i or j, later in the paper, indicates the background vector component. With magnetohydrostatic equilibrium for the background state, such that $\boldsymbol{u}_b = \boldsymbol{0}$, in the presence of an external gravity field $\boldsymbol{g}$, from Equation (2) we obtain

$$\frac{\partial}{\partial x_i}\left(p_b + \frac{B_{bj} B_{bj}}{2\mu_0}\right) - \frac{\partial}{\partial x_j}\left(\frac{B_{bi} B_{bj}}{\mu_0}\right) = \rho_b g_i. \qquad (7)$$

We then obtain the expression matching the right-hand side of Equation (3) by scalarly multiplying Equation (7) by $\boldsymbol{u}$ to yield

$$u_i \frac{\partial}{\partial x_i}\left(p_b + \frac{B_{bj} B_{bj}}{2\mu_0}\right) - u_i \frac{\partial}{\partial x_j}\left(\frac{B_{bi} B_{bj}}{\mu_0}\right) = \rho_b g_i u_i. \quad (8)$$

Subtracting Equations (7) and (8) from Equations (2) and (3), we derive the governing equations for the perturbations as

$$\frac{\partial \tilde{\rho}}{\partial t} + \frac{\partial}{\partial x_i}[(\rho_b + \tilde{\rho}) u_i] = 0, \qquad (9)$$

$$\frac{\partial[(\rho_b + \tilde{\rho}) u_i]}{\partial t} + \frac{\partial}{\partial x_j}[(\rho_b + \tilde{\rho}) u_i u_j] + \frac{\partial \tilde{p}_T}{\partial x_i}$$
$$- \frac{\partial}{\partial x_j}\left[\frac{\tilde{B}_i B_{bj} + B_{bi} \tilde{B}_j + \tilde{B}_i \tilde{B}_j}{\mu_0}\right] = \tilde{\rho} g_i, \quad (10)$$

$$\frac{\partial \tilde{e}}{\partial t} + \frac{\partial}{\partial x_i}[(e_b + \tilde{e}) u_i + \tilde{p}_T u_i]$$
$$- \frac{\partial}{\partial x_j}\left[\frac{\tilde{B}_i B_{bj} + B_{bi} \tilde{B}_j + \tilde{B}_i \tilde{B}_j}{\mu_0} u_i\right]$$
$$+ p_{bT} \frac{\partial u_j}{\partial x_j} - \frac{B_{bj} B_{bi}}{\mu_0} \frac{\partial u_i}{\partial x_j} = \tilde{\rho} g_i u_i (11)$$

$$\frac{\partial \tilde{B}_i}{\partial t} + \frac{\partial}{\partial x_j}\left[u_i (B_{bj} + \tilde{B}_j) - u_j (B_{bi} + \tilde{B}_i)\right] = 0_i, \quad (12)$$

$$\tilde{p}_T = (\gamma - 1)\left[\tilde{e} - \frac{(\rho_b + \tilde{\rho}) u_j u_j}{2}\right] - (\gamma - 2)\left[\frac{\tilde{B}_j B_{bj}}{\mu_0} + \frac{\tilde{B}_j \tilde{B}_j}{2\mu_0}\right], \qquad (13)$$

$$p_{bT} = (\gamma - 1) e_b - (\gamma - 2)\frac{B_{bj} B_{bj}}{2\mu_0}, \qquad (14)$$

$$\tilde{p} = (\gamma - 1)\left[\tilde{e} - \frac{(\rho_b + \tilde{\rho}) u_j u_j}{2} - \frac{\tilde{B}_j B_{bj}}{\mu_0} - \frac{\tilde{B}_j \tilde{B}_j}{2\mu_0}\right], \quad (15)$$

$$p_b = (\gamma - 1)\left[e_b - \frac{B_{bj} B_{bj}}{2\mu_0}\right]. \qquad (16)$$

2.3. *Magnetic Field Construction*

Our approach is to prescribe the magnetic field to model a flux tube or a set of flux tubes with structure approximating the observed magnetic field in the lower solar atmosphere. We place this field in a hydrostatic stratified atmosphere derived from the observed vertical profiles of the reference data. We

then adjust the plasma pressure and density distribution from the hydrostatic background as required to achieve magneto-hydrostatic equilibrium.

One approach to constructing the magnetic field is to apply a potential field to the prescribed atmosphere and allow the system to relax numerically (e.g., Solanki & Steiner 1990; Khomenko et al. 2008). Simulations of non-potential perturbations may then be applied to this equilibrium. For models utilizing very large data arrays, there may be considerable numerical overheads before the simulations can proceed, though it may be possible to circumvent this problem by using damping methods. It is conceivable that we may wish to investigate how small changes to the configuration effect energy transport mechanisms. With our analytic approach, these changes may be implemented almost instantaneously, and we can identify in advance exactly what changes are applied to the configuration. Using the potential method, the preliminary numerical relaxation must be completed and then the change to the configuration investigated. It is possible the potential method may be unsuitable for deriving background equilibrium multiple flux tube configurations. In this paper, we find no equilibrium exists for neighboring pairs of self-similar flux tubes in the absence of balancing forces. We are able to identify and calculate these forces.

We revisit the self-similarity method developed by Schlüter & Temesváry (1958) and applied variously for 2D (e.g., Deinzer 1965; Low 1980; Schüssler & Rempel 2005; Gordovskyy & Jain 2007; Fedun et al. 2011a; Shelyag et al. 2011) and to 3D solar magnetic configurations (Fedun et al. 2011b; Gent et al. 2013; Mumford et al. 2014). This represents one footpoint of a coronal loop or braid of loops. The other footpoint is presumed to be at a distance beyond the horizontal extent of our numerical domain. The arch of the loop occurs much higher in the corona than the vertical extent of our model (i.e., the loop has large aspect ratio), such that the flux tube may be regarded as vertically aligned.

The 3D magnetic field describing the configuration for a single open magnetic flux tube is denoted $^{m}\boldsymbol{B}_b$, where ^{m} indicates the mth flux tube in a magnetic field comprising more than one flux tube. To distinguish the index label for each magnetic flux tube configuration from other indices in this article, we use only labels $m, n \in \mathbb{N}$ and these appear as prefix superscripts. Summation convention does not apply to repetition of these indices. The model domain may reasonably be approximated in cylindrical polar coordinates, with radius measured from the axis of the flux tube, or in Cartesian coordinates, with x, y the local analogue of the longitudinal and latitudinal surface coordinates. The vertical coordinate z is aligned along the solar radius, with $z = 0$ at the base of the solar photosphere at $R_{\odot} \simeq 696\,\mathrm{Mm}$. We require an axially symmetric flux tube with its axis located at $(^{m}x, ^{m}y)$, expanding in radius with height z as the flux density reduces to balance the ambient plasma pressure.

In Cartesian coordinates the components of $^{m}\boldsymbol{B}_b$ are described by the self-similar relations

$$
\begin{aligned}
^{m}B_{bx} &= -\,^{m}S \frac{\partial \,^{m}f}{\partial x} \frac{\partial \,^{m}f}{\partial z}\,^{m}G, \\
^{m}B_{by} &= -\,^{m}S \frac{\partial \,^{m}f}{\partial y} \frac{\partial \,^{m}f}{\partial z}\,^{m}G, \\
^{m}B_{bz} &= \,^{m}S \left[\left(\frac{\partial \,^{m}f}{\partial x} \right)^2 + \left(\frac{\partial \,^{m}f}{\partial y} \right)^2 \right]\,^{m}G + b_{00}.
\end{aligned}
\tag{17}
$$

The sign ± 1 is indicated by ^{m}S to determine the orientation of the magnetic field along the mth flux tube. Real b_{00} is a constant, chosen to yield a weak ambient vertical field in which any flux tubes are situated.

$$
^{m}f = \,^{m}r B_{0z}, \tag{18}
$$

$$
^{m}G = \frac{2\ell}{\sqrt{\pi} f_0} \exp\left(-\frac{^{m}f^2}{f_0{}^2} \right), \tag{19}
$$

$$
^{m}r = \sqrt{(x - ^{m}x)^2 + (y - ^{m}y)^2}, \tag{20}
$$

where ^{m}r is the radial distance from the axis at $(^{m}x, ^{m}y)$ and with ^{m}G determining the radial width of the flux tube by a Gaussian centered at $(^{m}x, ^{m}y)$. In the normalization coefficient, an appropriate length scale ℓ is included with the scaling factor f_0, which are uniform for all flux tubes. The reduction in the vertical field strength along the flux tube axis is specified by

$$
B_{0z} = b_{01} \exp\left(-\frac{z}{z_1} \right) + b_{02} \exp\left(-\frac{z}{z_2} \right), \tag{21}
$$

with b_{01} and b_{02} assigning the typical axial field strength from the photosphere and from the lower corona, respectively. z_1 and z_2 are scaling lengths. In principle, these constants could differ between each flux tube, yielding stronger non-uniformity in the total field. Keeping B_{0z} uniform sufficiently simplifies the equations for an analytic solution. The final result retains significant asymmetry.

Applying these to Equation (17) we obtain the explicit form for the single magnetic flux tube as

$$
\begin{aligned}
^{m}B_{bx} &= -\,^{m}S(x - ^{m}x) B_{0z}\,^{m}G \frac{\partial B_{0z}}{\partial z}, \\
^{m}B_{by} &= -\,^{m}S(y - ^{m}y) B_{0z}\,^{m}G \frac{\partial B_{0z}}{\partial z}, \\
^{m}B_{bz} &= \,^{m}S B_{0z}{}^2\,^{m}G + b_{00}.
\end{aligned}
\tag{22}
$$

Observations (Chapter 3.5 in Mariska 1992; Schrijver & Title 2003) indicate the atmosphere outside the flux tubes includes a non-zero magnetic field in many parts of the chromosphere and, due to the local turbulence, is likely to be composed of very small-scale structures. However, at the scales of interest the structure of this weak field is not likely to be dynamically significant. For simplicity in satisfying the divergence free condition, a vertical magnetic field seems reasonable.

2.4. Plasma Pressure and Density

In magnetohydrostatic equilibrium a background atmosphere and magnetic field configuration must satisfy Equation (7), which may also be expressed as:

$$
\nabla p_b + \nabla \frac{|\boldsymbol{B}_b|^2}{2\mu_0} - (\boldsymbol{B}_b \cdot \nabla) \frac{\boldsymbol{B}_b}{\mu_0} - \rho_b g \hat{\boldsymbol{z}} = \boldsymbol{0}, \tag{23}
$$

where $\hat{\boldsymbol{z}}$ is the unit vector and only the global gravitational acceleration directed toward the solar origin is included. The magnetic tension is non-zero due to the curvature of the field lines and has opposite sign as it acts as a restoring force to the magnetic pressure. We know that the pressure is a scalar quantity, so by taking the curl of ∇p we obtain

$$
\nabla \times \nabla p_b = \boldsymbol{0} = \nabla \times \left(\rho_b g \hat{\boldsymbol{z}} + \frac{(\boldsymbol{B}_b \cdot \nabla) \boldsymbol{B}_b}{\mu_0} - \nabla \frac{|\boldsymbol{B}_b|^2}{2\mu_0} \right). \tag{24}
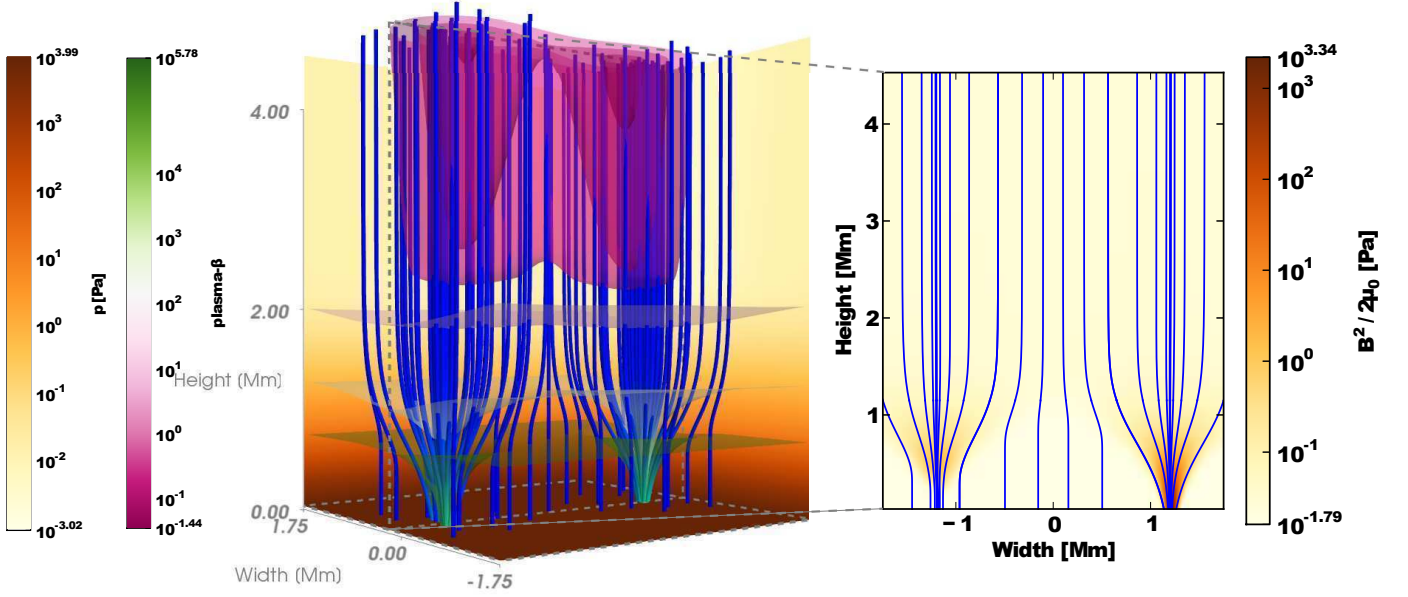$$

FIG. 2.— 3D-rendition of two flux tube pairs (left), indicative magnetic field lines plotted in blue against a background fill depicting thermal pressure at the rear and bottom planes. Isosurfaces indicate log plasma-β. Right: 2D-slice of magnetic pressure along $y = 0$ for the four flux tubes (i.e., two pairs) located at axes $(x, y) = (1.2, 0), (1.2, 0), (-1.15, 0.15), (-1.25, -0.15)$ Mm, indicative magnetic field lines overplotted in blue. The flux tube pair to the right share an identical axis at $(x, y) = (1.2, 0)$ Mm, while the axes to the left are slightly separated with respect to both the x and y directions. Note, the left pair have footpoints offset from $y = 0$, so the magnetic pressure on this slice is highest above the photosphere, where the flux tube pair expand and merge.

For a single flux tube, this condition is satisfied and a solution for p_b and ρ_b may be obtained similar to that outlined in Paper I.

We now adopt this approach for a pair of flux tubes whose magnetic configurations are denoted by ^mB_b and ^nB_b and the total background magnetic field $B_b = {}^mB_b + {}^nB_b$. Two pairs of such flux tubes, with pressure distribution derived as follows, are illustrated in Figure 2. Apart from the magnetic field lines, the plasma-β distribution also clearly indicates two distinct magnetic structures with low plasma-$\beta < 1$ in the lower corona and high plasma-$\beta > 1$ in the photosphere and chromosphere. Note plasma-$\beta \propto p/|B|^2$. To make a determination of the necessary pressure distribution for such an arrangement, it is useful to decompose the pressure and density into terms that are purely hydrostatic and independent of the magnetic field and terms that represent corrections to balance the effects of the flux tubes.

Those vertical profiles satisfying the purely hydrostatic background are denoted p_{bh} and ρ_{bh}, and are derived from the observed vertical profiles of Vernazza et al. (1981) and McWhirter et al. (1975) or similar, as described in Paper I.

Adjustment to the pressure distribution required to restore equilibrium due to the inclusion of the magnetic configurations ^mB_b and ^nB_b are denoted by $^mp_{bm}$, $^np_{bm}$, respectively, and by $^{mn}p_{bm}$ for their pairwise interaction. Hence, $p_b = p_{bh} + {}^mp_{bm} + {}^np_{bm} + {}^{mn}p_{bm}$. A corresponding decomposition of the density is also applied, using the same superscripts and subscripts. Equation (23), thus expanded, may then be arranged to yield

$$\nabla(p_{bh} + {}^mp_{bm} + {}^np_{bm} + {}^{mn}p_{bm}) = \quad (25)$$
$$[({}^mB_b + {}^nB_b) \cdot \nabla]\frac{({}^mB_b + {}^nB_b)}{\mu_0} - \nabla\frac{|{}^mB_b + {}^nB_b|^2}{2\mu_0}$$
$$+ (\rho_h + {}^m\rho_{bm} + {}^n\rho_{bm} + {}^{mn}\rho_{bm})g\hat{z}.$$

In this form, the curl of the right-hand side is not $\mathbf{0}$ for the self-similar magnetic field, as explained in Appendix A.1. In general, there is no valid scalar-field solution to Equation (25) for p_b. It makes physical sense that this should be so. Pairs of magnetic flux tubes in close proximity will be inclined to attract or repel, depending on their relative polarity, so that Equation (25) is not in equilibrium. Nevertheless, observational evidence exists of multiple flux tubes in relative stability (Dowdy et al. 1986; Solanki 1993; De Pontieu et al. 2003), suggesting the presence of some additional balancing forces. These may reside in local anomalies in the neighborhood density and pressure distributions, effects from events at some distance or forces acting at or below the footpoints. The nature and source of these forces is complex and beyond the scope of this article, but we conclude that an additional force term is required to satisfy Equation (25).

We can identify the net force acting in Equation (25) from the non-vanishing terms within the right-hand side of Equation (24). First, let us eliminate the terms, for which we already have solutions:

$$\nabla p_{bh} = \rho_{bh}g\hat{z} \quad \text{and}$$

and

$$\nabla {}^mp_{bm} = {}^m\rho_{bm}g\hat{z} - \nabla\frac{|{}^mB_b|^2}{2\mu_0} + ({}^mB_b \cdot \nabla)\frac{{}^mB_b}{\mu_0}.$$

The terms $^mp_{bm}$ and $^m\rho_{bm}$ are derived as in Paper I, taking into account the revised definition of the field in Equation (22). They are detailed in Equations (A19) and (A20) of Appendix A.2, and equivalently $^np_{bm}$ and $^n\rho_{bm}$.

This leaves only the interaction terms remaining of Equation (25) Then, having identified the non-vanishing terms in the right-hand side of Equation (24) from amongst these interaction terms, as detailed in Appendix A.1, we subtract them to
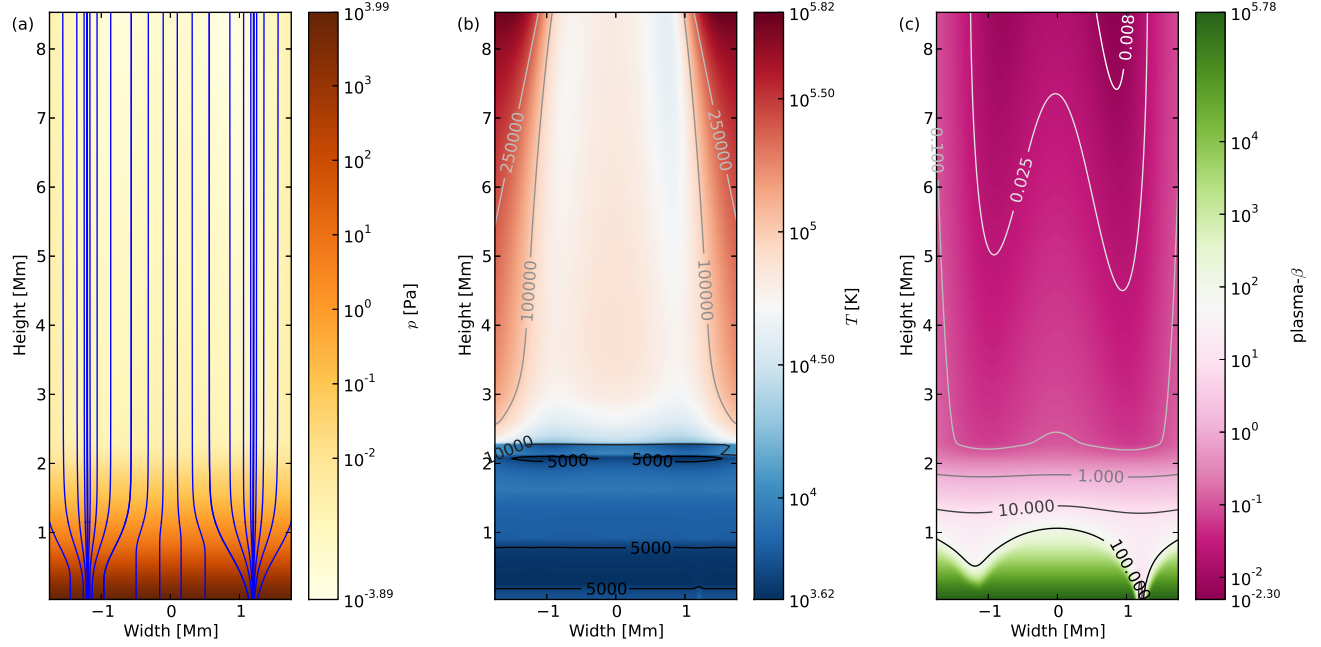
FIG. 3.— 2D slices along $y = 0$ of (a) thermal pressure with indicative magnetic field lines overplotted, and (b) temperature and (c) plasma beta with line contours overplotted, for flux tubes located at axes $(x, y) = (1.2, 0), (1.2, 0), (-1.15, 0.15), (-1.25, -0.15)$ Mm.

obtain

$$
\nabla^{mn}p_{b\mathrm{m}} = ({}^{m}\boldsymbol{B}_b \cdot \nabla)\frac{{}^{n}\boldsymbol{B}_b}{\mu_0} + ({}^{n}\boldsymbol{B}_b \cdot \nabla)\frac{{}^{m}\boldsymbol{B}_b}{\mu_0}
$$
$$
- \nabla\frac{({}^{m}\boldsymbol{B}_b \cdot {}^{n}\boldsymbol{B}_b)}{\mu_0} + {}^{mn}\rho_{b\mathrm{m}}\, g\hat{\boldsymbol{z}}
$$
$$
- \left(\frac{{}^{m}B_{bz}}{\mu_0}\frac{\partial {}^{n}B_{bx}}{\partial z} + \frac{{}^{n}B_{bz}}{\mu_0}\frac{\partial {}^{m}B_{bx}}{\partial z}\right)\hat{\boldsymbol{x}}
$$
$$
- \left(\frac{{}^{m}B_{bz}}{\mu_0}\frac{\partial {}^{n}B_{by}}{\partial z} + \frac{{}^{n}B_{bz}}{\mu_0}\frac{\partial {}^{m}B_{by}}{\partial z}\right)\hat{\boldsymbol{y}}, \quad (26)
$$

where $\hat{\boldsymbol{x}}$ and $\hat{\boldsymbol{y}}$ are unit vectors. Equation (26) may be solved by considering each vector component in turn:

$$
\frac{\partial {}^{mn}p_{b\mathrm{m}}}{\partial x} = \frac{{}^{m}B_{bx}}{\mu_0}\frac{\partial {}^{n}B_{bx}}{\partial x} + \frac{{}^{m}B_{by}}{\mu_0}\frac{\partial {}^{n}B_{bx}}{\partial y} + \frac{{}^{n}B_{bx}}{\mu_0}\frac{\partial {}^{m}B_{bx}}{\partial x}
$$
$$
+ \frac{{}^{n}B_{by}}{\mu_0}\frac{\partial {}^{m}B_{bx}}{\partial y} - \frac{\partial}{\partial x}\frac{({}^{m}\boldsymbol{B}_b \cdot {}^{n}\boldsymbol{B}_b)}{\mu_0},
$$

$$
\frac{\partial {}^{mn}p_{b\mathrm{m}}}{\partial y} = \frac{{}^{m}B_{bx}}{\mu_0}\frac{\partial {}^{n}B_{by}}{\partial x} + \frac{{}^{m}B_{by}}{\mu_0}\frac{\partial {}^{n}B_{by}}{\partial y} + \frac{{}^{n}B_{bx}}{\mu_0}\frac{\partial {}^{m}B_{by}}{\partial x}
$$
$$
+ \frac{{}^{n}B_{by}}{\mu_0}\frac{\partial {}^{m}B_{by}}{\partial y} - \frac{\partial}{\partial y}\frac{({}^{m}\boldsymbol{B}_b \cdot {}^{n}\boldsymbol{B}_b)}{\mu_0} \quad (27)
$$

and

$$
\frac{\partial {}^{mn}p_{b\mathrm{m}}}{\partial z} = \frac{{}^{m}B_{bx}}{\mu_0}\frac{\partial {}^{n}B_{bz}}{\partial x} + \frac{{}^{m}B_{by}}{\mu_0}\frac{\partial {}^{n}B_{bz}}{\partial y} + \frac{{}^{m}B_{bz}}{\mu_0}\frac{\partial {}^{n}B_{bz}}{\partial z}
$$
$$
+ \frac{{}^{n}B_{bx}}{\mu_0}\frac{\partial {}^{m}B_{bz}}{\partial x} + \frac{{}^{n}B_{by}}{\mu_0}\frac{\partial {}^{m}B_{bz}}{\partial y} + \frac{{}^{n}B_{bz}}{\mu_0}\frac{\partial {}^{m}B_{bz}}{\partial z}
$$
$$
+ {}^{mn}\rho_{b\mathrm{m}}g - \frac{\partial}{\partial z}\frac{({}^{m}\boldsymbol{B}_b \cdot {}^{n}\boldsymbol{B}_b)}{\mu_0}. \quad (28)
$$

The solution for ${}^{mn}p_{b\mathrm{m}}$ is specified by Equation (A21) and ${}^{mn}\rho_{b\mathrm{m}}$ by Equation (A22) and detailed in Appendix A.2. We

can now specify the background pressure and density profiles in the 3D space as $p_b = p_{b\mathrm{h}} + {}^{m}p_{b\mathrm{m}} + {}^{n}p_{b\mathrm{m}} + {}^{mn}p_{b\mathrm{m}}$ and $\rho_b = \rho_{b\mathrm{h}} + {}^{m}\rho_{b\mathrm{m}} + {}^{n}\rho_{b\mathrm{m}} + {}^{mn}\rho_{b\mathrm{m}}$. Note that numeric values of the last three terms in the expressions for p_b and ρ_b can be negative. A minimal constraint on the choice of parameters for the magnetic field configuration must be that both sums are sufficiently positive to guarantee that $p_b + \tilde{p} > 0$ and $\rho_b + \tilde{\rho} > 0$ everywhere while the system is being perturbed.

Figure 3 shows vertical slices of the pressure and temperature for two pairs of flux tubes as well as the resulting plasma-β. Two flux tubes exactly co-located on the right form a slightly stronger magnetic structure, while on the left, two identical flux tubes are slightly separated to form a weaker configuration. The delineation into two distinct combinations is most evident in the temperature and plasma-β distributions. The radial symmetry is broken and there is a clear opportunity to investigate the interaction between the flux tubes, although they are almost identical.

For more challenging configurations, we require more flux tubes with irregular spacing. First, we need to consider the consequences of this configuration for the MHD equations.

2.5. *Consequences for the MHD Equations*

In Section 2.4, we have derived profiles for the background pressure and plasma density. Suppose that p_b and ρ_b are now thus defined for the magnetic flux tube pair ${}^{1}\boldsymbol{B}_b$ and ${}^{2}\boldsymbol{B}_b$. If we subtract Equation (7) from the unperturbed Equation (2), as presented in Section 2.2, we then obtain

$$
\rho_b\frac{\partial u_i}{\partial t} = \frac{\partial}{\partial x_i}\left(p_b + \frac{B_{bj}B_{bj}}{2\mu_0}\right) - \frac{\partial}{\partial x_j}\left(\frac{B_{bi}B_{bj}}{\mu_0}\right) - \rho_b g_i
$$
$$
= -(\delta_{1i} + \delta_{2i})\left[\frac{{}^{1}B_{b3}}{\mu_0}\frac{\partial {}^{2}B_{bi}}{\partial x_3} + \frac{{}^{2}B_{b3}}{\mu_0}\frac{\partial {}^{1}B_{bi}}{\partial x_3}\right], \quad (29)
$$

where $(x_1, x_2, x_3) = (x, y, z)$ and δ_{ij} is the Kronecker delta and the latter equality arises from the supplementary terms

applying in Equation (26). That is, the system is out of equilibrium because the equality of Equation (7) is no longer valid for the multi-flux tube configuration. In this form the advective term from Equation (10) would also contribute, as $u_i \neq 0_i$ for the background state. However, by restoring equilibrium as follows, this term reverts to zero.
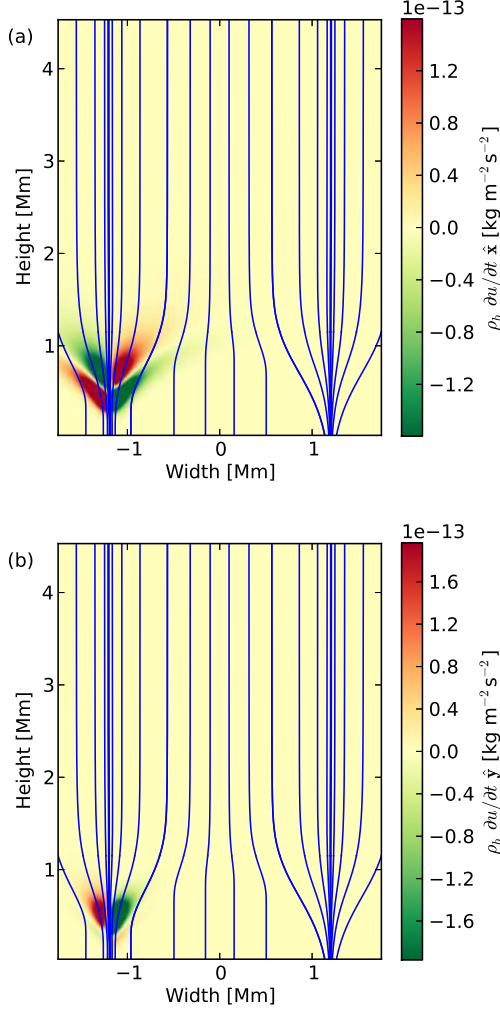

FIG. 4.— 2D slices along $y = 0$ of forces applying in Equation (30) for flux tubes at axes $(x, y) = (1.2, 0), (1.2, 0), (-1.15, 0.15), (-1.25, -0.15)$ Mm of the $\hat{\boldsymbol{x}}$-component (a) and $\hat{\boldsymbol{y}}$-component (b). Indicative magnetic field lines are overplotted in blue.

The x-component, Figure 4 panel (a), and the y-component, panel (b), of the net forces from Equation (29) applying along $y = 0$ for two pairs of flux tubes are illustrated. The pair of flux tubes on the right share an identical axis at $(x, y) = (1.2, 0)$ Mm, so the forces applying between them are zero on $y = 0$, whereas on the left the flux tube axes are slightly separated with respect to both the x and y directions. These forces are most evident in the chromosphere, where the field curvature is strongest. Alternating azimuthal trajectories of the forces with radius and height suggest that mutual torsional oscillations would result in the absence of any balancing forces. There are also forces acting between both pairs, but these are negligible near the footpoints because of the large axial separation and in the corona because of the weakness of the tension forces.

This magnetic field, with two flux tubes may be expressed as $\boldsymbol{B} = {}^1\boldsymbol{B}_b + {}^2\boldsymbol{B}_b + \tilde{\boldsymbol{B}}$. Thus, $|\boldsymbol{B}|^2 = |{}^1\boldsymbol{B}_b|^2 + |{}^2\boldsymbol{B}_b|^2 + |\tilde{\boldsymbol{B}}|^2 + 2\,{}^1\boldsymbol{B}_b \cdot \tilde{\boldsymbol{B}} + 2\,{}^2\boldsymbol{B}_b \cdot \tilde{\boldsymbol{B}} + 2\,{}^1\boldsymbol{B}_b \cdot {}^2\boldsymbol{B}_b$, with an equivalent pairwise decomposition also applying for the tension force $(\boldsymbol{B} \cdot \nabla)\boldsymbol{B}$. Hence, terms pertaining to interactions between a pair of background flux tubes ${}^1\boldsymbol{B}_b$ and ${}^2\boldsymbol{B}_b$ exclude the perturbations $\tilde{\boldsymbol{B}}$.

If we extend this to a network of N magnetic flux tubes with the configuration ${}^m\boldsymbol{B}_b$ as defined by Equation (22), but free to differ by axial location $({}^mx, {}^my)$, then the magnetic field can be expressed by the sum

$$\boldsymbol{B} = \boldsymbol{B}_b + \tilde{\boldsymbol{B}} = \left(\sum_{m=1}^{N} {}^m\boldsymbol{B}_b\right) + \tilde{\boldsymbol{B}},$$

and the restriction to pairwise interactions between each mth flux tube, its neighbors and the perturbed magnetic field still applies. The latter equality from Equation (29) can be generalized for N flux tubes to

$$\rho_b \frac{\partial \boldsymbol{u}}{\partial t} = \boldsymbol{F}_{\text{bal}} = -\sum_{m,n=1|m\neq n}^{N} \frac{{}^nB_{bz}}{\mu_0} \frac{\partial\,{}^mB_{bx}}{\partial z}\hat{\boldsymbol{x}} \quad (30)$$

$$-\sum_{m,n=1|m\neq n}^{N} \frac{{}^nB_{bz}}{\mu_0} \frac{\partial\,{}^mB_{by}}{\partial z}\hat{\boldsymbol{y}} + 0\hat{\boldsymbol{z}},$$

in which the explicit expression for each mn pairing is given in Equation (A10) of Appendix A.1. To satisfy the equality with $\rho\boldsymbol{g}$, Equation (7) must be revised to

$$\frac{\partial}{\partial x_i}\left(p_b + \frac{B_{bj}B_{bj}}{2\mu_0}\right) - \frac{\partial}{\partial x_j}\left(\frac{B_{bi}B_{bj}}{\mu_0}\right) - F_{\text{bal}i} = \rho_b g_i. \quad (31)$$

Scalar multiplication of Equation (30) with $\boldsymbol{u}$ then yields

$$\boldsymbol{F}_{\text{bal}}\cdot\boldsymbol{u} = -u_x \sum_{m,n=1|m\neq n}^{N} \frac{{}^nB_{bz}}{\mu_0} \frac{\partial\,{}^mB_{bx}}{\partial z} - u_y \sum_{m,n=1|m\neq n}^{N} \frac{{}^nB_{bz}}{\mu_0} \frac{\partial\,{}^mB_{by}}{\partial z} \quad (32)$$

and Equation (8) must also be revised as

$$u_i\frac{\partial}{\partial x_i}\left(p_b + \frac{B_{bj}B_{bj}}{2\mu_0}\right) - u_i\frac{\partial}{\partial x_j}\left(\frac{B_{bi}B_{bj}}{\mu_0}\right) - F_{\text{bal}i}u_i = \rho_b g_i u_i. \quad (33)$$

Now, subtracting Equation (31) from Equation (2) and Equation (33) from Equation (3), we obtain the revised MHD equations for the perturbed momentum and energy

$$\frac{\partial[(\rho_b + \tilde{\rho})u_i]}{\partial t} + \frac{\partial}{\partial x_j}\left[(\rho_b + \tilde{\rho})u_i u_j + \tilde{p}_T\right] \quad (34)$$

$$-\frac{\partial}{\partial x_j}\left[\frac{\tilde{B}_i B_{bj} + B_{bi}\tilde{B}_j + \tilde{B}_i\tilde{B}_j}{\mu_0}\right] + F_{\text{bal}i} = \tilde{\rho}g_i,$$

$$\frac{\partial \tilde{e}}{\partial t} + \frac{\partial}{\partial x_j}\left[(e_b + \tilde{e})u_j - \frac{\tilde{B}_i\tilde{B}_j}{\mu_0}u_i + \tilde{p}_T u_j\right] \quad (35)$$

$$-\frac{\partial}{\partial x_j}\left[\frac{\tilde{B}_i B_{bj} + B_{bi}\tilde{B}_j}{\mu_0}u_i\right]$$

$$+p_{bT}\frac{\partial u_j}{\partial x_j} - \frac{B_{bj}B_{bi}}{\mu_0}\frac{\partial u_i}{\partial x_j} + F_{\text{bal}i}u_i = \tilde{\rho}g_i u_i.$$

With the addition of $\boldsymbol{F}_{\mathrm{bal}}$ in Equation (34) the unperturbed system has

$$\rho_b \frac{\partial \boldsymbol{u}}{\partial t} = \boldsymbol{0}.$$

Note also that this does not affect any terms depending on the perturbations and is independent of changes to the perturbed system, so it remains constant over time and the background is in equilibrium.

The corresponding term $\boldsymbol{F}_{\mathrm{bal}} \cdot \boldsymbol{u}$ in Equation (35) is zero in the steady state, but is apparently subject to amplification by horizontal components of the velocity field. However, an equal and opposite effect is present due to the subtraction of the other terms in Equation (33), so these combine to result in zero net energy effect.

2.6. *Inhomogeneous Multiple Flux Tubes*

As outlined in Section 2.5, when adding multiple flux tubes, the background magnetic pressure gradient and tension force are fully specified by the sum of single and pairwise interactions between each flux tube. Thus, given a magnetic field comprising N magnetic flux tubes,

$$\boldsymbol{B}_b = \sum_{m=1}^{N} {}^{m}\boldsymbol{B}_b, \tag{36}$$

$$p_b = p_{b\mathrm{h}} + \sum_{m=1}^{N} {}^{m}p_{b\mathrm{m}} + \sum_{m,n=1|n>m}^{N} {}^{mn}p_{b\mathrm{m}} \tag{37}$$

and

$$\rho_b = \rho_{b\mathrm{h}} + \sum_{m=1}^{N} {}^{m}\rho_{b\mathrm{m}} + \sum_{m,n=1|n>m}^{N} {}^{mn}\rho_{b\mathrm{m}}, \tag{38}$$

in which ${}^{mn}p_{b\mathrm{m}}$ and ${}^{mn}\rho_{b\mathrm{m}}$ represent the action of ${}^{m}\boldsymbol{B}_b$ on ${}^{n}\boldsymbol{B}_b$ *and vice versa*. Hence, the inequality under the summation is required for this quantity to be counted only once for each pair of flux tubes.

The time-independent momentum equation describing the background equilibrium is then

$$\rho_b g \hat{\boldsymbol{z}} - \nabla p_b - \nabla \frac{|\boldsymbol{B}_b|^2}{2\mu_0} + \frac{(\boldsymbol{B}_b \cdot \nabla)\boldsymbol{B}_b}{\mu_0} + \boldsymbol{F}_{\mathrm{bal}} = \boldsymbol{0}, \tag{39}$$

where $\boldsymbol{F}_{\mathrm{bal}}$ is as specified by Equation (30). Note that this solution will yield a different equilibrium configuration to the solution of Equation (23) (Section 2.4), valid for a single flux tube. Consider some single flux tube with $\boldsymbol{F}_{\mathrm{bal}} \equiv \boldsymbol{0}$. Let us construct an identical flux tube by combining some field configurations with a common axis of the form ${}^{m}\boldsymbol{B}_b$, then $\boldsymbol{F}_{\mathrm{bal}}$ will be non-zero. Therefore, the solution of Equation (23) for the single flux tube will obtain different distributions for pressure and density to a solution of Equation (39) for an identical magnetic field, with the former equilibrium satisfying Equation (10) and the latter Equation (34).

We have devised a background magnetic field construction by the summation of multiple locally defined field configurations in magnetohydrostatic equilibrium with the stratified atmosphere, spanning the transition between the solar photosphere and lower solar corona. Let us consider some opportunities presented by this arrangement.
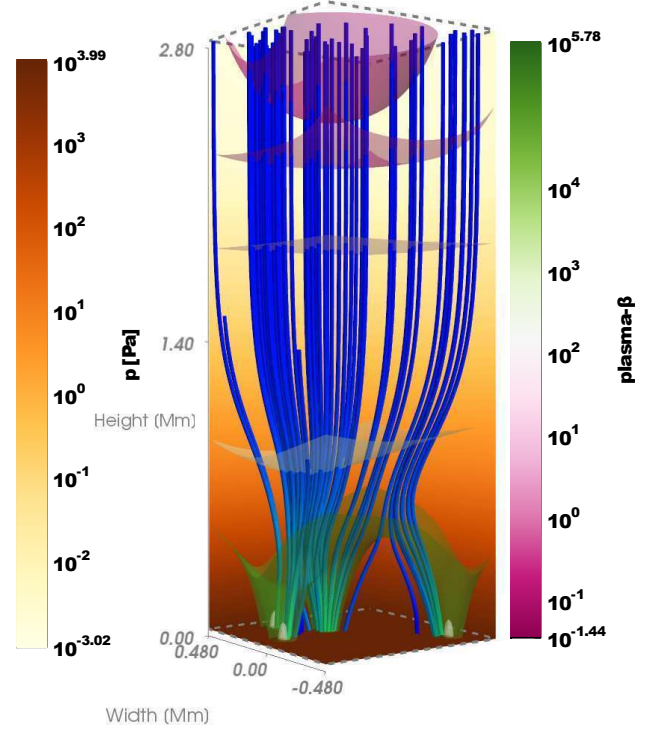

FIG. 5.— Magnetic field comprising flux tube sources with independent axes located at $(x, y) = (0.34, 0.20)$, $(-0.31, -0.34)$, $(0.07, 0.33)$ and $(0.14, 0.04)$ Mm. Sample magnetic field lines are overplotted in blue and isosurfaces indicate the variation in plasma-β. Background fill shows thermal pressure on those planes.

On scales below the minimum observable resolution, the fine structure of the magnetic field can add to the complexity and dynamics of a magnetic flux tube. We combine four independent magnetic sources clustered within a photospheric surface element $1" \times 1" \approx 725\,\mathrm{km} \times 725\,\mathrm{km}$. This corresponds to the maximum resolution for the magnetic field observations of, for example, the Helioseismic and Magnetic Imager of the Solar Dynamics Observatory (Kosovichev & HMI Science Team 2007). Hence, the fine structure of a magnetic field configuration below this resolution would be treated as a single flux tube, but may well be, and most likely is, the combination of an irregular magnetic field network.

We thus construct a non-axisymmetric background magnetic field, which, in the corona, forms a single identifiable structure, but in the chromosphere has significant complexity. Although the field lines merge in the corona, they retain complexity in the form of pressure, density, and plasma-β fluctuations. An example of such an arrangement is illustrated in Figure 5. Perturbations to this steady background will be subject to nonlinear effects in the horizontal direction, due to the irregular field strength, and also in the vertical direction, due to the pressure gradient and the transition from the high to low plasma-β regime.

For the same field configuration a 2D horizontal slice at $z = 0.5\,\mathrm{Mm}$ of the steady background thermal pressure profile is shown in Figure 7. The deviations in the plasma pressure are small compared to the vertical differential. Overplotted in blue are some magnetic field lines. As might be expected, field lines emanate from the flux tube axes, indicated by the light (low pressure regions). Above the three footpoint
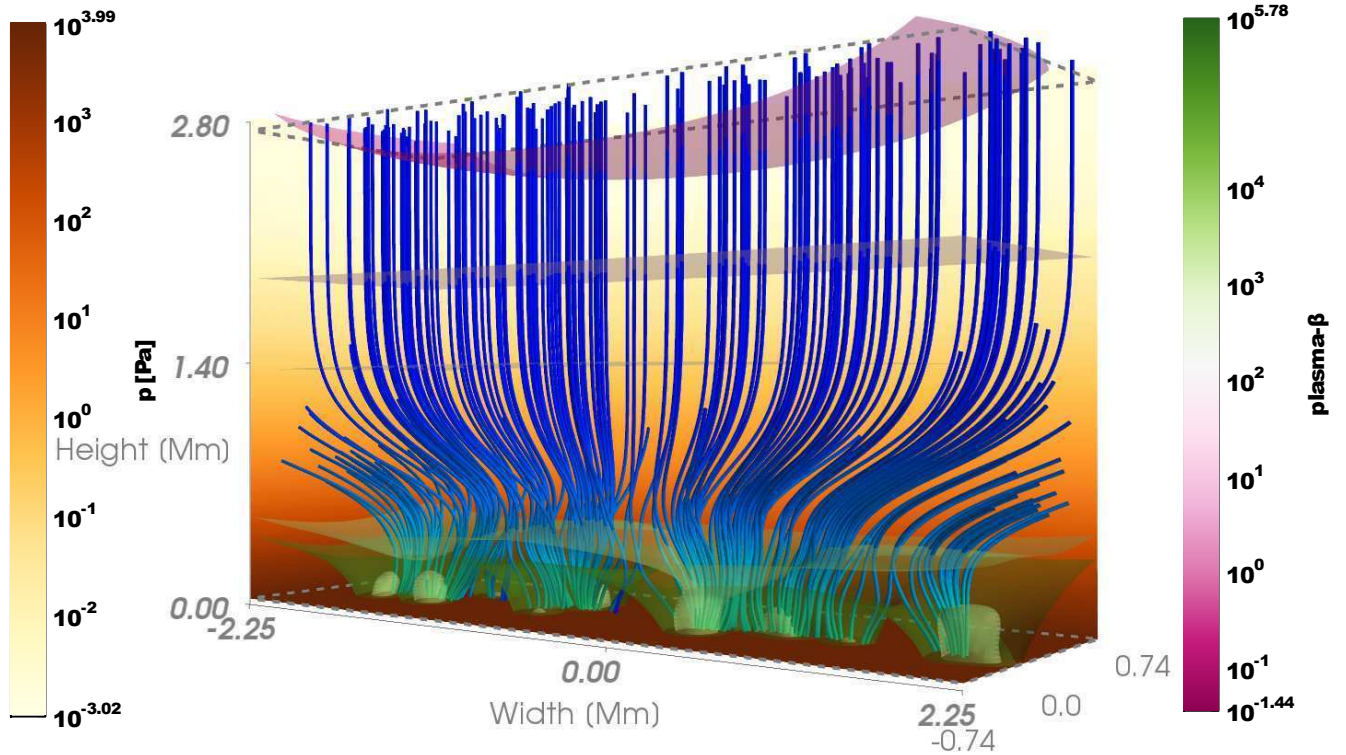
FIG. 6.— Example of magnetic field configuration modeling granular lanes within the photosphere. Multiple flux tubes emerging through the chromosphere along a narrow lane merge in the corona to form a magnetic canopy.

axes located at the photosphere in the positive x, y quadrant the pressure has already merged into a single depression.
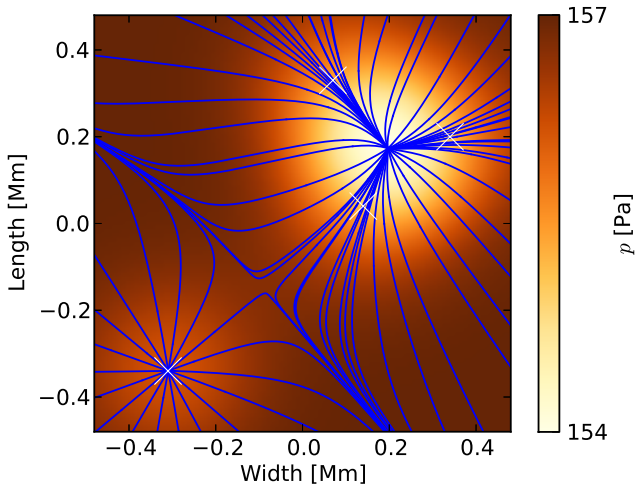

FIG. 7.— 2D horizontal slice of thermal pressure at $z = 0.5\,\mathrm{Mm}$ for the magnetic field comprising flux tube sources with photospheric footpoint axes independently located at $(x, y) = (0.34, 0.20)$, $(-0.31, -0.34)$, $(0.07, 0.33)$ and $(0.14, 0.04)\,\mathrm{Mm}$, as identified in the figure by white crosses. Due to radial expansion, by $z \geq 0.5\,\mathrm{Mm}$ the three flux tubes in the positive quadrant have merged. Indicative horizontal magnetic field lines are overplotted in blue, diverted where the flux tubes intersect.

By the height of the TR, the smaller depression within

the flux tube anchored to the photosphere at $(x, y) = (-0.31, -0.34)\,\mathrm{Mm}$ also merges with the other three to form a single, non-uniform low pressure core inside the composite magnetic flux tube. In the plane field lines are not purely radial, with azimuthal trajectories appearing due to the influence of neighboring flux tubes. Between the axis at $(-0.31, -0.34)\,\mathrm{Mm}$ and the other three axes field lines with opposite polarity appear to meet, and in the regions between the three positive axes there are high concentrations of field lines as they merge with each other. In 3D, these lines do not meet due to the vertical component of the field. However magneto-acoustic waves along these converging field lines may interfere with each other near these intersections.

In ideal MHD there is no mechanism for reconnection. For numerical stability, however, simulations require a minimum level of numerical diffusion. Such diffusion will be strongest in regions where the field lines converge, resulting in topological changes to the field configuration analogous to magnetic reconnection.

In addition to providing an interesting structure for a single flux tube as in the preceding example, it is possible to construct networks of flux tubes on larger scales. Figure 6 illustrates a 3D rendition of the magnetic field resembling a granular lane. This could be extended to form a ring or other network of flux tubes. With a sufficiently large numerical domain, the horizontal interactions in the corona between flux tubes and networks of flux tubes can be explored. Even in the corona, on this scale the field can exhibit much more anisotropy.
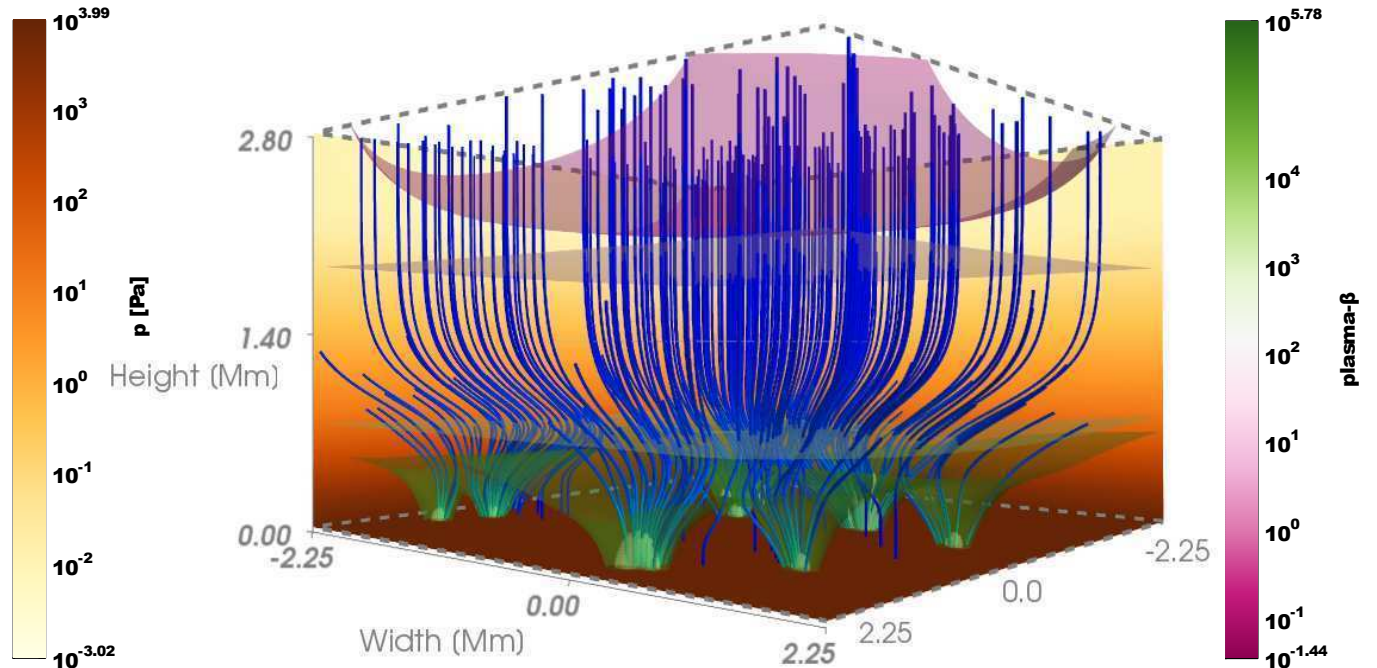
FIG. 8.— Example of magnetic field configuration modeling an active region with multiple magnetic bright points and emerging flux tubes. The strong compact individual magnetic flux tubes in the chromosphere spread with height and merge to fill the corona.

In Figure 8, we display an environment resembling a solar active region comprising a multitude of magnetic bright points with flux tubes emerging from the photosphere. Although the magnetic field spreads out to fill the corona, the merger is far from uniform and this presents an opportunity to explore the dynamics between, and within, neighboring flux tubes.

All of these examples are in magnetohydrostatic equilibrium for the stratified solar atmosphere, with positive plasma pressure and density throughout and low plasma-β in the corona, while for $z \lesssim 1\,\mathrm{Mm}$ plasma-$\beta \gg 1$.

Typical footpoint field strength for each flux tube is near $100\,\mathrm{mT}$, but varies depending on the number and proximity of neighboring flux tubes. Care in the field construction is required, with respect to the vertical and radial expansion factors, footpoint strength and axial proximity. The magnetic field strength should not become so high as to require plasma pressure or density to be negative in order to satisfy the pressure balance.

3. SUMMARY AND DISCUSSION

We have solved analytically the time-independent MHD equation of momentum for a configuration of multiple open magnetic flux tubes in magnetohydrostatic equilibrium embedded within a solar stratified atmosphere, with realistic parameters for plasma pressure, density, temperature, and magnetic field strength. The equilibrium is maintained through inclusion of appropriate horizontal balancing forces, which we have also identified and calculated. It may be argued that inclusion even of an appropriate choice of balancing forces undermines the relationship between $\boldsymbol{B}$, p and ρ, permitting any arbitrary atmosphere to be constructed. This would negate comparison with the real solar atmosphere. However, in our model the atmosphere is also constrained by observational comparison. We restrict the balancing forces to be the minimal requirement to solve the system, and so the atmospheric adjustments remain largely determined by the applied mag-

netic field.

This is a significant advance in achieving realistic modeling of the magnetized solar atmosphere. The solutions may also have application in other astrophysical environments, such as sunspots or magnetized atmosphere in gas giants. This advances the possibilities for analysis and numerical simulation of systems with background equilibria or quasi-equilibria. In particular, the existence of non-axisymmetric inhomogeneous configurations facilitates research of non-linear interactions between neighboring flux tubes. The presence of converging field lines between flux tubes may lead to interesting dynamics.

The model extends from the solar photosphere to the solar corona, incorporating the temperature minimum and the TR. There is some scale-independence to the model, in the sense that it could apply to a single flux tube emerging from a magnetic bright point or to more extended surface areas including flux tube networks in an active solar region. In the smaller scales, such as magnetic bright points, the flux tubes environment is far from force free.

There are two important analytical results. We have identified a sufficient condition to have a force-free steady solution for a magnetic field configuration subject to external vertical gravitation, as specified in Equation (A6) Appendix A.1

$$\frac{\partial B_x}{\partial y} = \frac{\partial B_y}{\partial x} \quad \text{and} \quad \frac{\partial B_z}{\partial y}\frac{\partial B_x}{\partial z} = \frac{\partial B_z}{\partial x}\frac{\partial B_y}{\partial z}.$$

This result is consistent with that of Low (1985), applying a general magnetic field of the form

$$\boldsymbol{B} = \left(\frac{\partial \phi}{\partial x}, \frac{\partial \phi}{\partial y}, \psi\right),$$

where ϕ and ψ are scalar functions. The former condition in Equation (A6) is immediately satisfied, and the latter is equiv-

alently specified by

$$\frac{\partial^2 \phi}{\partial x \partial z}\frac{\partial \psi}{\partial y} = \frac{\partial^2 \phi}{\partial y \partial z}\frac{\partial \psi}{\partial x},$$

for which the general solution is $\psi(x,y,z) = \Psi(z, \partial\phi/\partial z)$. This leads to the general solution of Low (1985) for the plasma pressure of the form

$$p + \frac{1}{2\mu_0}\Psi^2 - \frac{1}{\mu_0}\int^{\partial\phi/\partial z}\Psi(z,u)\,\mathrm{d}u = p_0(z). \quad (40)$$

$p_0(z)$ is an arbitrary function (p_{bh} in our model). The term under the integral is typically non-linear without a ready analytic solution. Low (1985) found a particular solution with $\Psi = \alpha\partial\phi/\partial z$. Summing magnetic structures, as we have done in Section 2.6, Low (1985) constructed a non-axisymmetric multi-nodal configuration.

In our model

$$\phi = \frac{^mSf_0{}^2}{2B_{0z}}\frac{\partial B_{0z}}{\partial z}\,{}^mG \text{ and } \psi = {}^mSB_{0z}{}^2\,{}^mG + b_{00} \neq \alpha\partial\phi/\partial z,$$
$$(41)$$

so that, for the single flux tube, our model yields a new explicit solution to Equation (40). The general solution of Low (1985) requires Equation (A6) be satisfied for Equation (23), i.e., force-free. We have not verified whether this is a necessary condition, such that failure to satisfy this condition would exclude the possibility of a force-free steady solution. Here we introduce a new set of explicit solutions, applicable when the latter condition in Equation (A6) is satisfied for the net magnetic forces applying to Equation (39). These solutions allow general configurations for the magnetic field. Superpositions of various magnetic field configurations may be combined. Provided the former equality in Equation (A6) is satisfied for each individual configuration, an analytic solution to Equation (39) exists for p_b and ρ_b, with $\boldsymbol{F}_{\mathrm{bal}}$ minimally defined by Equation (30).

Note that the former equality in Equation (A6) is equivalent to the condition $J_z = 0$, the vertical component of background current density and corresponds to an untwisted magnetic field configuration. Our background field is not current-free. In the axisymmetric model, applying for the single flux tube, the background current is purely azimuthal. For the multiple flux tubes, the background horizontal current includes radial and azimuthal components. Let us stress that this does not exclude J_z for the perturbed system.

Low (1985) took the approach of identifying the conditions in Equation (A6) and constructing a magnetic field to satisfy these. His solution was applied to an exponential model background pressure, which approximates a coronal atmosphere. Our approach is to seek a construction for the magnetic field, which is sufficiently flexible to adapt to the observed magnetic structures and which matches the more realistic solar atmosphere modeled by Vernazza et al. (1981) and McWhirter et al. (1975), and would permit an analytic solution. We are motivated by physical considerations, such as controlling the radial expansion of the flux tubes distinctly for the chromosphere and for the corona. Therefore, the latter condition in Equation (A6) has been used to identify those terms, which can only be accommodated by including balancing forces. Although we approximate the magnetized background atmosphere as steady, both of these approaches have limitations. Particularly, in the chromosphere the atmosphere

is neither static nor force free. Many other physical forces may play a significant role, such as radiation, partial ionization effects and thermal conduction. Nevertheless, this is a considerable advance toward modeling effectively some part of this complex and dynamic system.

For our self-similar flux tube model, we have verified that it is not possible to construct a field of neighboring flux tubes with a steady solution in the absence of balancing forces. These forces can be identified and calculated, so that the background be in quasi-equilibrium. It would be interesting to investigate whether this approach could be extended to magnetic fields with twist, such that the former condition in Equation (A6) is not satisfied, but that balancing forces might yet be identified.

An alternative approach could be to extend the analysis of Low (1985) and seek a magnetic field that satisfies completely Equation (A6) by construction. From the solenoidal condition

$$\frac{\partial^2 \phi}{\partial x^2} + \frac{\partial^2 \phi}{\partial y^2} + \frac{\partial}{\partial z}\left(f(z)\frac{\partial \phi}{\partial z}\right) \quad (42)$$

we seek a solution with f and ϕ in a form that may be adapted to match the observed magnetic structures of the solar atmosphere. Finding such a solution is a considerable challenge and there is no guarantee that such configurations should realistically model open flux tubes or loops. While we will consider this approach in the future, it is well beyond the current aims: the construction of currently observable complex loop structures with the ultimate goal of investigating *wave propagation* and *wave energy transport/coupling* in such complex systems. It is not our intention here to model loop or active region dynamics, which involve evolution of the background due to processes, such as reconnection, field relaxation, etc.

In this article, we have restricted our examples to systems of open flux tubes of the same polarity. In Appendix A, the derivation is also valid for solutions involving opposite polarity. Indeed, the constants ^mS need not be identical, taking any set of real values subject to the constraint that plasma pressure and density remain physical. This could add further curvature for the magnetic field to the non-trivial field curvature that this article describes between flux tubes. A further, though very challenging, improvement would be to include torsional components to the flux tubes, with $B_\phi \neq 0$.

Simulations using alternate steady background configurations with single and multiple flux tubes, will help identify the extent to which the interactions between magnetic flux tubes amplify or dampen the transport of energy in the lower solar atmosphere. Also analytical investigation of the various equilibrium conditions could advance our understanding of the structure and forces acting in this solar region.

APPENDIX

SOLUTION TO BACKGROUND STATIC EQUILIBRIUM

Non-vanishing Terms in the Curl of ∇p

If we consider Equation (24) for a general magnetic field $\boldsymbol{B}$ subject to gravity acting only along the vertical direction, we require

$$\nabla \times \nabla P = \nabla \times \left(\rho g \hat{\boldsymbol{z}} + \frac{(\boldsymbol{B} \cdot \nabla) \boldsymbol{B}}{\mu_0} - \nabla \frac{|\boldsymbol{B}|^2}{2\mu_0} \right) = \boldsymbol{0}. \tag{A1}$$

On the left-hand side the pressure is a scalar, so this term vanishes. The magnetic pressure term as a scalar also has vanishing curl, so for the magnetic tension and gravitation we require

$$\frac{\partial}{\partial y} \left[(\boldsymbol{B} \cdot \nabla) \frac{B_z}{\mu_0} + \rho g \right] - \frac{\partial}{\partial z} \left[(\boldsymbol{B} \cdot \nabla) \frac{B_y}{\mu_0} \right] = \qquad 0, \tag{A2}$$

$$\frac{\partial}{\partial z} \left[(\boldsymbol{B} \cdot \nabla) \frac{B_x}{\mu_0} \right] - \frac{\partial}{\partial x} \left[(\boldsymbol{B} \cdot \nabla) \frac{B_z}{\mu_0} + \rho g \right] = \qquad 0, \tag{A3}$$

$$\frac{\partial}{\partial x} \left[(\boldsymbol{B} \cdot \nabla) \frac{B_y}{\mu_0} \right] - \frac{\partial}{\partial y} \left[(\boldsymbol{B} \cdot \nabla) \frac{B_x}{\mu_0} \right] = \qquad 0. \tag{A4}$$

From Equation (A4) we obtain

$$\frac{\partial}{\partial x} \left[(\boldsymbol{B} \cdot \nabla) B_y \right] - \frac{\partial}{\partial y} \left[(\boldsymbol{B} \cdot \nabla) B_x \right] = 0 \Rightarrow \left[\boldsymbol{B} \cdot \nabla - \frac{\partial B_z}{\partial z} \right] \left(\frac{\partial B_y}{\partial x} - \frac{\partial B_x}{\partial y} \right) + \frac{\partial B_z}{\partial x} \frac{\partial B_y}{\partial z} - \frac{\partial B_z}{\partial y} \frac{\partial B_x}{\partial z} = 0. \tag{A5}$$

A solution to Equation (A5) exists if

$$\frac{\partial B_x}{\partial y} = \frac{\partial B_y}{\partial x} \quad \text{and} \quad \frac{\partial B_z}{\partial y} \frac{\partial B_x}{\partial z} = \frac{\partial B_z}{\partial x} \frac{\partial B_y}{\partial z} \tag{A6}$$

Equation (A6) is a sufficient condition to satisfy Equation (A4). Differentiating Equation (A2) with respect to x and Equation (A3) with respect to y and then summing them, we are left only with the z-derivative of Equation (A5). Again we obtain the relations in Equation (A6) as a sufficient condition to fully satisfy Equation (A1). Indeed, this may be a necessary condition for a steady magnetic field within a vertical gravity field (Gabriel 1976; Gibson & Low 1998), but we have not verified this.

In the case of the self-similar construction for a single flux tube defined by Equation (22), both conditions in Equation (A6) are satisfied. However, for a pair of flux tubes denoted by $^m\boldsymbol{B}_b$ and $^n\boldsymbol{B}_b$, where $x_i \neq x_j$ or $y_i \neq y_j$, the latter condition in Equation (A6) is not satisfied for the cross terms

$$\frac{\partial\,^m B_{bz}}{\partial y} \frac{\partial\,^n B_{bx}}{\partial z} \neq \frac{\partial\,^m B_{bz}}{\partial x} \frac{\partial\,^n B_{by}}{\partial z}. \tag{A7}$$

In general configurations of vertical flux tube pairs may include derivative terms for which $y_i x_j \neq x_i y_j$, failing to satisfy Equation (A6). We have not identified an alternative construction in which this pairwise interaction can satisfy Equation (A6). It may be that for an asymmetric field magnetohydrostatic equilibrium cannot exist in the absence of balancing forces, but we have not verified this.

From Equation (A7) the non-vanishing terms in Equation (A1) can be identified. A sufficient requirement to equate the right-hand side to $\boldsymbol{0}$ will thus be to include a balancing force inside the brackets

$$- \frac{^m B_{bz}}{\mu_0} \frac{\partial\,^n B_{bx}}{\partial z} \hat{\boldsymbol{x}} - \frac{^n B_{bz}}{\mu_0} \frac{\partial\,^m B_{bx}}{\partial z} \hat{\boldsymbol{x}} - \frac{^m B_{bz}}{\mu_0} \frac{\partial\,^n B_{by}}{\partial z} \hat{\boldsymbol{y}} - \frac{^n B_{bz}}{\mu_0} \frac{\partial\,^m B_{by}}{\partial z} \hat{\boldsymbol{y}}. \tag{A8}$$

It follows that it is sufficient to modify the interaction terms in Equation (25) to

$$\nabla\,^{mn} p_{bm} + \nabla \left(^m\boldsymbol{B}_b \cdot \frac{^n\boldsymbol{B}_b}{\mu_0} \right) - \left(\frac{^m\boldsymbol{B}_b}{\mu_0} \cdot \nabla \right) {}^n\boldsymbol{B}_b - \left(\frac{^n\boldsymbol{B}_b}{\mu_0} \cdot \nabla \right) {}^m\boldsymbol{B}_b \tag{A9}$$

$$+ \frac{^m B_{bz}}{\mu_0} \frac{\partial\,^n B_{bx}}{\partial z} \hat{\boldsymbol{x}} + \frac{^n B_{bz}}{\mu_0} \frac{\partial\,^m B_{bx}}{\partial z} \hat{\boldsymbol{x}} + \frac{^m B_{bz}}{\mu_0} \frac{\partial\,^n B_{by}}{\partial z} \hat{\boldsymbol{y}} + \frac{^n B_{bz}}{\mu_0} \frac{\partial\,^m B_{by}}{\partial z} \hat{\boldsymbol{y}} - {}^{mn} \rho_{bm} g \hat{\boldsymbol{z}} = \boldsymbol{0}.$$

In this form we can now follow Appendix A.2 to solve for p and ρ. With plasma pressure and density thus modified, the equality in Equation (23) for the pressure balance is no longer valid. This will be restored by adding to the right-hand side the sum of forces $^{mn}\boldsymbol{F}$ matching the net force applying on $^n\boldsymbol{B}_b$ due to $^m\boldsymbol{B}_b$. Explicitly

$$^{mn}\boldsymbol{F} = - \frac{^m B_{bz}}{\mu_0} \frac{\partial\,^n B_{bx}}{\partial z} \hat{\boldsymbol{x}} - \frac{^m B_{bz}}{\mu_0} \frac{\partial\,^n B_{by}}{\partial z} \hat{\boldsymbol{y}} \tag{A10}$$

$$= \left[\frac{(x - {}^n x)\hat{\boldsymbol{x}} + (y - {}^n y)\hat{\boldsymbol{y}}}{\mu_0} \right] {}^n S\,^n G \left[{}^m S B_{0z}{}^2\,{}^m G + b_{00} \right] \left[\left(1 - \frac{2\,{}^n f^2}{f_0{}^2} \right) \left(\frac{\partial B_{0z}}{\partial z} \right)^2 + B_{0z} \frac{\partial^2 B_{0z}}{\partial z^2} \right]$$

Plasma Pressure and Density Adjustment

Basic Quantities and Derivatives

Listed here are the various derivatives from the expressions for a single flux tube, which will be required in the calculations.

$$\frac{\partial\,^m f}{\partial x} = \frac{(x - \,^m x)B_{0z}}{^m r}, \quad \frac{\partial\,^m f}{\partial y} = \frac{(y - \,^m y)B_{0z}}{^m r}, \quad \frac{\partial\,^m f}{\partial z} = \,^m r\frac{\partial B_{0z}}{\partial z}, \quad \frac{\partial\,^m G}{\partial\,^m f} = -\frac{2\,^m f\,^m G}{f_0^{\,2}},$$

$$\frac{\partial\,^m G}{\partial x} = -\frac{2(x - \,^m x)B_{0z}^{\,2}\,^m G}{f_0^{\,2}}, \quad \frac{\partial\,^m G}{\partial y} = -\frac{2(y - \,^m y)B_{0z}^{\,2}\,^m G}{f_0^{\,2}}, \quad \frac{\partial\,^m G}{\partial z} = -\frac{2\,^m f\,^m G\,^m r}{f_0^{\,2}}\frac{\partial B_{0z}}{\partial z}.$$

We will require the derivatives in these expressions as follows:

$$\frac{\partial\,^m B_{bx}}{\partial x} = \,^m S\,^m G\left(\frac{2(x - \,^m x)^2 B_{0z}^{\,3}}{f_0^{\,2}} - B_{0z}\right)\frac{\partial B_{0z}}{\partial z} \tag{A11}$$

$$\frac{\partial\,^m B_{bx}}{\partial y} = \frac{\partial\,^m B_{by}}{\partial x} = \frac{2\,^m S(x - \,^m x)(y - \,^m y)B_{0z}^{\,3}\,^m G}{f_0^{\,2}}\frac{\partial B_{0z}}{\partial z} \tag{A12}$$

$$\frac{\partial\,^m B_{bx}}{\partial z} = \,^m S(x - \,^m x)\,^m G\left(\frac{2\,^m f^2}{f_0^{\,2}} - 1\right)\frac{\partial B_{0z}}{\partial z}^{\,2} - \,^m S(x - \,^m x)B_{0z}\,^m G\frac{\partial^2 B_{0z}}{\partial z^2} \tag{A13}$$

$$\frac{\partial\,^m B_{by}}{\partial y} = \,^m S\,^m G\left(\frac{2(y - \,^m y)^2 B_{0z}^{\,3}}{f_0^{\,2}} - B_{0z}\right)\frac{\partial B_{0z}}{\partial z} \tag{A14}$$

$$\frac{\partial\,^m B_{by}}{\partial z} = \,^m S(y - \,^m y)\,^m G\left(\frac{2\,^m f^2}{f_0^{\,2}} - 1\right)\frac{\partial B_{0z}}{\partial z}^{\,2} - \,^m S(y - \,^m y)B_{0z}\,^m G\frac{\partial^2 B_{0z}}{\partial z^2} \tag{A15}$$

$$\frac{\partial\,^m B_{bz}}{\partial x} = -\,^m S\frac{2(x - \,^m x)B_{0z}^{\,4}\,^m G}{f_0^{\,2}}, \tag{A16}$$

$$\frac{\partial\,^m B_{bz}}{\partial y} = -\,^m S\frac{2(y - \,^m y)B_{0z}^{\,4}\,^m G}{f_0^{\,2}}, \tag{A17}$$

$$\frac{\partial\,^m B_{bz}}{\partial z} = 2\,^m S B_{0z}\,^m G\left(1 - \frac{^m f^2}{f_0^{\,2}}\right)\frac{\partial B_{0z}}{\partial z} \tag{A18}$$

Balancing Plasma Pressure and Density for Single Flux Tube

Each single flux tube in isolation as prescribed by Equation (22) has axial symmetry. For convenience we retrace the solution in cylindrical coordinates as described in Paper I, but here applying a constant vertical ambient background field. We also include the constant $^m S = \pm 1$, allowing alternative polarity to be considered for each flux tube.

$$\begin{aligned}
\frac{\partial\,^m p_{bm}}{\partial r} &= -\frac{\partial}{\partial r}\frac{|^m\boldsymbol{B}_b|^2}{2\mu_0} + \frac{^m B_{br}}{\mu_0}\frac{\partial\,^m B_{br}}{\partial r} + \frac{^m B_{bz}}{\mu_0}\frac{\partial\,^m B_{br}}{\partial z} \\
&= -\frac{\partial}{\partial r}\frac{|^m\boldsymbol{B}_b|^2}{2\mu_0} + \frac{\partial}{\partial r}\frac{^m B_{br}^2}{2\mu_0} - \frac{(^m S B_{0z}^{\,2}\,^m G + b_{00})}{\mu_0}\frac{\partial}{\partial z}\left(^m S\,^m r B_{0z}\,^m G\frac{\partial B_{0z}}{\partial z}\right) \\
&= -\frac{\partial}{\partial r}\frac{^m B_{bz}^2}{2\mu_0} - \frac{^m S^2 B_{0z}\,^m f\,^m G^2}{\mu_0}\left(\frac{\partial B_{0z}}{\partial z}\right)^2 + \frac{2\,^m S^2 B_{0z}\,^m f^3\,^m G^2}{\mu_0 f_0^{\,2}}\left(\frac{\partial B_{0z}}{\partial z}\right)^2 - \frac{^m S b_{00}\,^m f\,^m G}{\mu_0}\frac{\partial^2 B_{0z}}{\partial z^2} \\
&\quad + \left[\frac{2\,^m S b_{00}\,^m f^3\,^m G}{\mu_0 B_{0z} f_0^{\,2}} - \frac{^m S b_{00}\,^m f\,^m G}{\mu_0 B_{0z}}\right]\left(\frac{\partial B_{0z}}{\partial z}\right)^2 - \frac{^m S^2 B_{0z}^{\,2}\,^m f\,^m G^2}{\mu_0}\frac{\partial^2 B_{0z}}{\partial z^2} \\
&= -\frac{\partial}{\partial r}\frac{^m B_{bz}^2}{2\mu_0} - \frac{^m S^2}{2\mu_0}\frac{\partial}{\partial r}\left(^m f\,^m G\frac{\partial B_{0z}}{\partial z}\right)^2 + \frac{\partial}{\partial r}\left(\frac{^m S^2 B_{0z} f_0^{\,2}\,^m G^2}{4\mu_0}\frac{\partial^2 B_{0z}}{\partial z^2}\right) \\
&\quad + \frac{\partial}{\partial r}\left(\frac{^m S b_{00} f_0^{\,2}\,^m G}{2\mu_0 B_{0z}}\frac{\partial^2 B_{0z}}{\partial z^2}\right) - \frac{\partial}{\partial r}\left(\frac{^m S b_{00}\,^m f^2\,^m G}{\mu_0 B_{0z}^{\,2}}\left[\frac{\partial B_{0z}}{\partial z}\right]^2\right) - \frac{\partial}{\partial r}\left(\frac{^m S b_{00} f_0^{\,2}\,^m G}{2\mu_0 B_{0z}^{\,2}}\left[\frac{\partial B_{0z}}{\partial z}\right]^2\right).
\end{aligned}$$

Integrating with respect to r we obtain a solution for ${}^m p_{b\mathrm{m}}$ as

$$
{}^m p_{b\mathrm{m}} = -\frac{|{}^m\boldsymbol{B_b}|^2}{2\mu_0} - \frac{{}^m S b_{00}\,{}^m G}{\mu_0 B_{0z}{}^2}\left[{}^m f^2 + \frac{f_0{}^2}{2}\right]\left(\frac{\partial B_{0z}}{\partial z}\right)^2 + \frac{{}^m S^2 B_{0z} f_0{}^2\,{}^m G^2}{4\mu_0}\frac{\partial^2 B_{0z}}{\partial z^2} + \frac{{}^m S b_{00} f_0{}^2\,{}^m G}{2\mu_0 B_{0z}}\frac{\partial^2 B_{0z}}{\partial z^2}. \quad \text{(A19)}
$$

This must be matched by the solution obtained by solving the z-component of the pressure balance equation so

$$
{}^m p_{b\mathrm{m}} = \int {}^m\rho_{b\mathrm{m}} g\,\mathrm{d}z - \frac{{}^m B_{br}^2}{2\mu_0} + \int \frac{{}^m B_{br}}{\mu_0}\frac{\partial\,{}^m B_{bz}}{\partial r}\,\mathrm{d}z = -\frac{{}^m B_{bz}^2}{2\mu_0} + \int \frac{{}^m B_{bz}}{\mu_0}\frac{\partial\,{}^m B_{br}}{\partial z}\,\mathrm{d}r
$$

$$
\Rightarrow {}^m\rho_{b\mathrm{m}} g = \frac{\partial}{\partial z}\frac{{}^m B_{br}^2}{2\mu_0} - \frac{\partial}{\partial z}\frac{{}^m B_{bz}^2}{2\mu_0} - \frac{{}^m B_{br}}{\mu_0}\frac{\partial\,{}^m B_{bz}}{\partial r} + \frac{\partial}{\partial z}\int \frac{{}^m B_{bz}}{\mu_0}\frac{\partial\,{}^m B_{br}}{\partial z}\,\mathrm{d}r
$$

$$
{}^m\rho_{b\mathrm{m}} g = \frac{\partial}{\partial z}\left(\frac{{}^m S^2\,{}^m f^2\,{}^m G^2}{2\mu_0}\left[\frac{\partial B_{0z}}{\partial z}\right]^2 - \frac{{}^m S^2 B_{0z}{}^4\,{}^m G^2}{2\mu_0}\right) - \frac{\partial}{\partial z}\left(\frac{{}^m S b_{00} B_{0z}{}^2\,{}^m G}{\mu_0}\right)
$$

$$
- \frac{\partial}{\partial z}\left(\frac{{}^m S^2\,{}^m f^2\,{}^m G^2}{2\mu_0}\left[\frac{\partial B_{0z}}{\partial z}\right]^2\right) + \frac{\partial}{\partial z}\left(\frac{{}^m S^2 B_{0z} f_0{}^2\,{}^m G^2}{4\mu_0}\frac{\partial^2 B_{0z}}{\partial z^2} + \frac{{}^m S b_{00} f_0{}^2\,{}^m G}{2\mu_0 B_{0z}}\frac{\partial^2 B_{0z}}{\partial z^2}\right)
$$

$$
- \frac{\partial}{\partial z}\left(\frac{{}^m S b_{00}\,{}^m G}{\mu_0 B_{0z}{}^2}\left({}^m f^2 + \frac{f_0{}^2}{2}\right)\left[\frac{\partial B_{0z}}{\partial z}\right]^2\right) + \frac{{}^m S^2\,{}^m f\,{}^m G}{\mu_0}\frac{\partial B_{0z}}{\partial z}\frac{\partial}{\partial r}\left(B_{0z}{}^2\,{}^m G\right)
$$

$$
{}^m\rho_{b\mathrm{m}} = \frac{{}^m S^2\,{}^m G^2}{\mu_0 g}\left(\frac{f_0{}^2}{4} - {}^m f^2\right)\frac{\partial B_{0z}}{\partial z}\frac{\partial^2 B_{0z}}{\partial z^2} - \frac{3\,{}^m S b_{00}\,{}^m G}{\mu_0 g B_{0z}{}^2}\left(\frac{f_0{}^2}{2} + {}^m f^2\right)\frac{\partial B_{0z}}{\partial z}\frac{\partial^2 B_{0z}}{\partial z^2}
$$

$$
+ \left[\frac{{}^m S b_{00}\,{}^m G}{\mu_0 g B_{0z}{}^3}\left(\frac{2\,{}^m f^4}{f_0{}^2} + f_0{}^2 + {}^m f^2\right)\right]\left[\frac{\partial B_{0z}}{\partial z}\right]^3 + \frac{2\,{}^m S b_{00} B_{0z}\,{}^m G}{\mu_0 g}\left(\frac{{}^m f^2}{f_0{}^2} - 1\right)\frac{\partial B_{0z}}{\partial z}
$$

$$
+ \left[\frac{{}^m S^2 B_{0z} f_0{}^2\,{}^m G^2}{4\mu_0 g} + \frac{{}^m S b_{00} f_0{}^2\,{}^m G}{2\mu_0 g B_{0z}}\right]\frac{\partial^3 B_{0z}}{\partial z^3} - \frac{2\,{}^m S^2 B_{0z}{}^3\,{}^m G^2}{\mu_0 g}\frac{\partial B_{0z}}{\partial z}. \quad \text{(A20)}
$$

The distribution for the plasma density can therefore be obtained by dividing Equation (A20) by g. For our example we apply a constant g for simplicity due to the small variation over the vertical domain of our model, but the solution is equally valid with variable gravity $g = g(z)$. However, it is not suitable for including self-gravity due to the horizontal fluctuations in the plasma density. This would arguably be very small in comparison to the global solar gravity for the scales we are considering.

Plasma Pressure and Density from Pairwise Interactions

We require ${}^{mn} p_{b\mathrm{m}}$, the pressure deviation in response to the force exerted by flux tube configuration ${}^m\boldsymbol{B}_b$ on ${}^n\boldsymbol{B}_b$ and vice versa. Taking advantage of the equality in Equation (A12) the y-derivatives in Equation (27) can be transposed and the tension terms cancel directly to yield

$$
\frac{\partial\,{}^{mn} p_{b\mathrm{m}}}{\partial x} = -\frac{\partial}{\partial x}\left(\frac{{}^m\boldsymbol{B}_b \cdot {}^n\boldsymbol{B}_b}{\mu_0}\right) + \frac{{}^m B_{bx}}{\mu_0}\frac{\partial\,{}^n B_{bx}}{\partial x} + \frac{{}^n B_{bx}}{\mu_0}\frac{\partial\,{}^m B_{bx}}{\partial x} + \frac{{}^m B_{by}}{\mu_0}\frac{\partial\,{}^n B_{by}}{\partial x} + \frac{{}^n B_{by}}{\mu_0}\frac{\partial\,{}^m B_{by}}{\partial x}
$$

$$
= -\frac{\partial}{\partial x}\left(\frac{{}^m B_{bz}\,{}^n B_{bz}}{\mu_0}\right).
$$

Integrating with respect to x we thus obtain

$$
{}^{mn} p_{b\mathrm{m}} = -\frac{{}^m B_{bz}\,{}^n B_{bz}}{\mu_0} \quad \text{(A21)}
$$

plus an arbitrary function constant in x. Solving Equation (27) for the y-component recovers the identical solution, so any additional terms can have only z-dependence and are fully accounted for within the hydrostatic background terms $p_{b\mathrm{h}}$ and $\rho_{b\mathrm{h}}$. The solution to Equation (28) must also match so

$$
{}^{mn} p_{b\mathrm{m}} = \int {}^{mn}\rho_{b\mathrm{m}} g + ({}^m\boldsymbol{B}_b \cdot \nabla)\frac{{}^n B_{bz}}{\mu_0} + ({}^n\boldsymbol{B}_b \cdot \nabla)\frac{{}^m B_{bz}}{\mu_0}\,\mathrm{d}z - \frac{{}^m\boldsymbol{B}_b \cdot {}^n\boldsymbol{B}_b}{\mu_0} = -\frac{{}^m B_{bz}\,{}^n B_{bz}}{\mu_0}
$$

$$
\Rightarrow {}^{mn}\rho_{b\mathrm{m}} g = \frac{\partial}{\partial z}\left(\frac{{}^m B_{bx}\,{}^n B_{bx}}{\mu_0}\right) + \frac{\partial}{\partial z}\left(\frac{{}^m B_{by}\,{}^n B_{by}}{\mu_0}\right) - ({}^m\boldsymbol{B}_b \cdot \nabla)\frac{{}^n B_{bz}}{\mu_0} - ({}^n\boldsymbol{B}_b \cdot \nabla)\frac{{}^m B_{bz}}{\mu_0}
$$

$$\mu_0 \, {}^{mn}\rho_{bm} g = \frac{\partial}{\partial z}\left({}^mS\,{}^nS(x - {}^mx)(x - {}^nx)\,{}^mG\,{}^nG\left[B_{0z}\frac{\partial B_{0z}}{\partial z}\right]^2 \right) - \frac{\partial}{\partial z}\left({}^mB_{bz}\,{}^nB_{bz}\right) - {}^mB_{bx}\frac{\partial\,{}^nB_{bz}}{\partial x}$$

$$+ \frac{\partial}{\partial z}\left({}^mS\,{}^nS(y - {}^my)(y - {}^ny)\,{}^mG\,{}^nG\left[B_{0z}\frac{\partial B_{0z}}{\partial z}\right]^2 \right) - {}^mB_{by}\frac{\partial\,{}^nB_{bz}}{\partial y} - {}^nB_{bx}\frac{\partial\,{}^mB_{bz}}{\partial x} - {}^nB_{by}\frac{\partial\,{}^mB_{bz}}{\partial y}$$

$$\ldots = 2\,{}^mS\,{}^nS(x - {}^mx)(x - {}^nx)B_{0z}\,{}^mG\,{}^nG\left[\frac{\partial B_{0z}}{\partial z}\right]^3 + 2\,{}^mS\,{}^nS(x - {}^mx)(x - {}^nx)B_{0z}{}^2\,{}^mG\,{}^nG\frac{\partial B_{0z}}{\partial z}\frac{\partial^2 B_{0z}}{\partial z^2}$$

$$- 2\,{}^mS\,{}^nS(x - {}^mx)(x - {}^nx)B_{0z}\frac{{}^mf^2}{f_0{}^2}\,{}^mG\,{}^nG\left[\frac{\partial B_{0z}}{\partial z}\right]^3 - 2\,{}^mS\,{}^nS(x - {}^mx)(x - {}^nx)B_{0z}\frac{{}^nf^2}{f_0{}^2}\,{}^mG\,{}^nG\left[\frac{\partial B_{0z}}{\partial z}\right]^3$$

$$+ 2\,{}^mS\,{}^nS(y - {}^my)(y - {}^ny)B_{0z}\,{}^mG\,{}^nG\left[\frac{\partial B_{0z}}{\partial z}\right]^3 + 2\,{}^mS\,{}^nS(y - {}^my)(y - {}^ny)B_{0z}{}^2\,{}^mG\,{}^nG\frac{\partial B_{0z}}{\partial z}\frac{\partial^2 B_{0z}}{\partial z^2}$$

$$\begin{aligned}
{}^{mn}\rho_{bm} = &\frac{2}{\mu_0 g}\,{}^mS\,{}^nS(x - {}^mx)(x - {}^nx)B_{0z}\,{}^mG\,{}^nG\left[\frac{f_0{}^2 - {}^mf^2 - {}^nf^2}{f_0{}^2}\left(\frac{\partial B_{0z}}{\partial z}\right)^3 + B_{0z}\frac{\partial B_{0z}}{\partial z}\frac{\partial^2 B_{0z}}{\partial z^2}\right] \\
&+ \frac{2}{\mu_0 g}\,{}^mS\,{}^nS(y - {}^my)(y - {}^ny)B_{0z}\,{}^mG\,{}^nG\left[\frac{f_0{}^2 - {}^mf^2 - {}^nf^2}{f_0{}^2}\left(\frac{\partial B_{0z}}{\partial z}\right)^3 + B_{0z}\frac{\partial B_{0z}}{\partial z}\frac{\partial^2 B_{0z}}{\partial z^2}\right] \\
&+ \frac{2}{\mu_0 g}\,{}^mS\,{}^nS B_{0z}{}^3\,{}^mG\,{}^nG\frac{\partial B_{0z}}{\partial z}\left[\frac{B_{0z}{}^2\,({}^nx - {}^mx)^2}{f_0{}^2} + \frac{B_{0z}{}^2\,({}^ny - {}^ny)^2}{f_0{}^2} - 2\right] \\
&+ \frac{2}{\mu_0 g}b_{00}B_{0z}\frac{\partial B_{0z}}{\partial z}\left[\frac{{}^mS\,{}^mG\,{}^mf^2}{f_0{}^2} - {}^mS\,{}^mG + \frac{{}^nS\,{}^nG\,{}^nf^2}{f_0{}^2} - {}^nS\,{}^nG\right].
\end{aligned} \tag{A22}$$

REFERENCES

Aschwanden, M. J. 2005, Physics of the Solar Corona. An Introduction with Problems and Solutions (2nd edition)
Aschwanden, M. J., Schrijver, C. J., & Alexander, D. 2001, ApJ, 550, 1036
De Pontieu, B., Tarbell, T., & Erdélyi, R. 2003, ApJ, 590, 502
DeForest, C. E. 2007, ApJ, 661, 532
Deinzer, W. 1965, ApJ, 141, 548
Dowdy, Jr., J. F., Rabin, D., & Moore, R. L. 1986, Sol. Phys., 105, 35
Erdélyi, R. 2008, in IAU Symposium, Vol. 247, Physics of the Sun and its Atmosphere, ed. B. N. Dwivedi & U. Narain (Cambridge: Cambridge University Press), 61–108
Fedun, V., Erdélyi, R., & Shelyag, S. 2009, Sol. Phys., 258, 219
Fedun, V., Shelyag, S., & Erdélyi, R. 2011a, ApJ, 727, 17
Fedun, V., Verth, G., Jess, D. B., & Erdélyi, R. 2011b, ApJ, 740, L46
Gabriel, A. H. 1976, Royal Society of London Philosophical Transactions Series A, 281, 339
Gent, F. A., Fedun, V., Mumford, S. J., & Erdélyi, R. 2013, MNRAS, 435, 689
Gibson, S. E., & Low, B. C. 1998, ApJ, 493, 460
Gordovskyy, M., & Jain, R. 2007, ApJ, 661, 586
Hasan, S. S., & van Ballegooijen, A. A. 2008, ApJ, 680, 1542
Hasan, S. S., van Ballegooijen, A. A., Kalkofen, W., & Steiner, O. 2005, ApJ, 631, 1270
Hunter, J. D. 2007, Computing In Science & Engineering, 9, 90
Jeffrey, N. L. S., & Kontar, E. P. 2013, ApJ, 766, 75
Jess, D. B., McAteer, R. T. J., Mathioudakis, M., et al. 2007, A&A, 476, 971
Jones, E., Oliphant, T., Peterson, P., & Others. 2001, SciPy: Open source scientific tools for Python, http://www.scipy.org/
Khomenko, E., & Collados, M. 2012, ApJ, 747, 87
Khomenko, E., Collados, M., & Felipe, T. 2008, Sol. Phys., 251, 589
Klimchuk, J. A. 2006, Sol. Phys., 234, 41
Kontar, E. P., Hannah, I. G., & MacKinnon, A. L. 2008, A&A, 489, L57
Kosovichev, A. G., & HMI Science Team. 2007, Astronomische Nachrichten, 328, 339
Levine, R. H., & Withbroe, G. L. 1977, Sol. Phys., 51, 83

López Fuentes, M. C., Démoulin, P., & Klimchuk, J. A. 2008, ApJ, 673, 586
Low, B. C. 1980, Sol. Phys., 67, 57
—. 1985, ApJ, 293, 31
—. 1988, ApJ, 330, 992
Malherbe, J. M., Schmieder, B., Ribes, E., & Mein, P. 1983, A&A, 119, 197
Mariska, J. T. 1992, The Solar Transition Region (Cambridge Cambridge University Press)
McGuire, J. P., Tandberg-Hanssen, E., Krall, K. R., et al. 1977, Sol. Phys., 52, 91
McWhirter, R. W. P., Thonemann, P. C., & Wilson, R. 1975, A&A, 40, 63
Morton, R. J., Verth, G., Jess, D. B., et al. 2012, NatCo, 3, 1315
Mumford, S. J., Fedun, V., & Erdélyi, R. 2014, ArXiv e-prints, arXiv:1305.7415v2
Priest, E. R. 2000, Solar Magnetohydrodynamics (Dordrecht: D. Reidel)
Schlüter, A., & Temesváry, S. 1958, in IAU Symposium, Vol. 6, Electromagnetic Phenomena in Cosmical Physics, ed. B. Lehnert (Cambridge: Cambridge University Press), 263
Schrijver, C. J., & Title, A. M. 2003, ApJ, 597, L165
Schüssler, M., & Rempel, M. 2005, A&A, 441, 337
Shelyag, S., Fedun, V., & Erdélyi, R. 2008, A&A, 486, 655
Shelyag, S., Fedun, V., Keenan, F. P., Erdélyi, R., & Mathioudakis, M. 2011, Annales Geophysicae, 29, 883
Shelyag, S., Zharkov, S., Fedun, V., Erdélyi, R., & Thompson, M. J. 2009, A&A, 501, 735
Solanki, S. K. 1993, Space Sci. Rev., 63, 1
Solanki, S. K., & Steiner, O. 1990, A&A, 234, 519
Tsinganos, K., & Low, B. C. 1989, ApJ, 342, 1028
Vernazza, J. E., Avrett, E. H., & Loeser, R. 1981, ApJS, 45, 635
Verth, G., Goossens, M., & He, J.-S. 2011, ApJ, 733, L15
Vigeesh, G., Fedun, V., Hasan, S. S., & Erdélyi, R. 2012, ApJ, 755, 18
Wedemeyer-Böhm, S., Scullion, E., Steiner, O., et al. 2012, Nature, 486, 505
Winebarger, A. R., Warren, H. P., & Mariska, J. T. 2003, ApJ, 587, 439
Zirker, J. B. 1993, Sol. Phys., 148, 43
Zwaan, C. 1978, Sol. Phys., 60, 213